The National University of Science and Technology Politehnica Bucharest

Doctoral School of Electrical Engineering

OPTIMAL REACTIVE POWER CONTROL WITHIN A MICROGRID BASED ON PHOTOVOLTAIC POWER PLANTS

SUMMARY

PhD supervisor:
Emeritus Prof Dr. Eng. Valentin NĂVRĂPESCU

PhD student:
Eng. Mihai BURLACU

Bucharest
2024

CONTENTS

List of abbreviations **3**

Introduction **4**

Chapter 1. Photovoltaic power plants **6**

1.1. Basic notions 6

1.2. Photovoltaic cells 6

1.2.1. Materials 6

1.2.2. Electrical characterization of photovoltaic cell 6

1.2.3. Efficiency of photovoltaic systems 6

1.2.4. Estimation of the performance of photovoltaic systems 6

1.3. The concept of dispersed generation 7

1.3.1. Premises for the development of dispersed generation 7

1.3.2. Characteristics of dispersed generation 7

1.3.3. Classification of dispersed sources 7

1.4. Connection diagrams of dispersed sources 8

Chapter 2. Microgrids load flow **8**

2.1. Modeling of the elements of the electrical network 8

2.1.1. Electrical lines 8

2.1.2. Electrical Transformers 9

2.1.3. Loads and Distributed Sources 9

2.1.4. Capacitor Banks and Compensating Inductors 10

2.2. Load flow calculation 10

2.2.1. Basics of Load flow calculation 10

2.2.2. Backward-Forward Sweep Method 10

2.2.3. Advantages of Backward-Forward Sweep Method 13

2.3. Load flow calculation software 13

2.3.1. Presentation of the calculation software 13

2.3.2. Validation of the calculation software 15

Chapter 3. Integration of photovoltaic power plants into optimal reactive power control **15**

3.1. Formulation of the optimization problem 15

3.1.1. Objective function 15
3.1.2. Equality and inequality constraints 16
3.1.3. Model adaptations for metaheuristic algorithms 17
3.2. Metaheuristic optimization algorithms 18
3.2.1. General terms 18
3.2.2. Grey Wolf Optimizer 18
3.2.3. Genetic algorithms 19
3.2.4. Particle Swarm Optimization 20
3.2.5. Sine-Cosine Algorithm 20
3.2.6. Salp Swarm Algorithm 20
3.3. Case study 20
3.3.1. Microgrid studied 20
3.3.2. Comparison of metaheuristic algorithms 21
3.3.3. Integrating CEF into reactive power control 22
Chapter 4. Optimal reactive power control exclusively based on photovoltaic power plants 24
4.1. Strategies for PVPP reactive power control 24
4.1.1. Constant power factor 25
4.1.2. Local compensation of reactive power 25
4.1.3. Optimal reactive power control 26
4.2. Studied microgrid 27
4.3. Analysis of the operation of the microgrid 27
4.3.1. 16th of May 27
4.3.2. 6th of June 30
4.3.3. 26th of June 31
4.3.4. 9th of April 32
4.3.5. Analysis of the operation during one year 32
Chapter 5. Conclusions 33
5.1. General conclusions 33
5.2. Personal contributions 35
5.3. Further research proposals 36
Selective bibliography 36

LIST OF ABBREVIATIONS

In this paper, the following abreviations are used:

- CCP – Common Coupling Point;
- EDN – Electrical Distribution Networks;
- EPS – Electrical Power System;
- ETN – Electricity Transmission Networks;
- GA – Algoritm Genetic;
- GWO –Grey Wolf Optimization;
- HPP– Hydro-electric power plant;
- HV – High Voltage;
- LV – Low Voltage;
- MV – Medium Voltage;
- NPP– Nuclear-electric power plant;
- PSO –Particle Swarm Optimization;
- PVPP – Photovoltaic Power Plant;
- RES – Renewable Energy Sources;
- SCA –Sine-Cosine Algorithm;
- SSA –Salp Swarm Algorithm;
- TPP – Thermo-electric power plant.

INTRODUCTION

Optimizing the operation of electrical distribution networks is a relatively broad field, which includes a considerable number of applications, which generally aim to improve their efficiency and reliability and reduce operating and investment costs. To this end, optimization problems can be formulated both for the design stage and in the operating process, and for solving these problems a multitude of methods are available based either on mathematical algorithms or classical optimization techniques.

The main categories of challenges encountered in optimizing the expansion of electricity distribution networks can be divided into three main categories, depending on their nature: technical, economic and legislative.

From an economic point of view, the main challenge arises from the need to ensure a balance between increasing investment costs and reducing operating costs. Thus, it is necessary to find a compromise in order to keep investment costs at reasonable values while ensuring operational safety and achieving the lowest possible operating costs.

The extension of power grids from a technical point of view can consist of a variety of applications such as choosing the power lines to be built, sizing them, choosing electrical transformers and sizing them and selecting the equipment to be installed. It is also possible to determine the optimal location and sizing of equipment that contributes to increasing the efficiency of the network such as electricity storage systems, reactive power compensation, etc. The main criteria that are pursued, from a technical point of view, are the reduction of active power losses, the increase of reliability and safety in operation, the improvement of the voltage level and the stability of the network.

In addition to the technical and economic challenges, there are also a number of legislative regulations that can have a major influence in optimizing the expansion of the distribution network. For example, regulations relating to environmental impact, social impact or different eligibility criteria for accessing financial incentives can be added.

Within the process of operating electrical distribution networks, optimization problems aim to coordinate existing control devices to achieve one of the following objectives: minimizing active power losses, maximizing the level of reliability or stability of the network, optimizing the voltage level, etc.

For these purposes, optimal coordination is achieved between the controllable devices in the network, which are briefly presented below. A first category of controllable devices is represented by renewable sources that can contribute to voltage control through the reactive power generated, or distributed sources based on classic fuels, such as gas or diesel, which can also contribute by regulating the active power generated. The second category of controllable devices is represented by controllable consumers who accept, for certain periods of time, that some of their devices are disconnected or that certain devices are put into operation when it is convenient also from the point of view of the network. Thus, a flattening of the load curve or a consumption schedule can be achieved during periods when renewable sources also produce at the highest possible capacity. There are also devices to compensate for the reactive power required by consumers, such as capacitor banks or systems based on power electronics, such as

D-SVC or D-STATCOM. In recent times, there has been a significant increase in the number of electric vehicles charging stations in distribution systems, which can also be integrated as controllable devices in optimizing the operation of power grids. To this end, the charging of electric vehicles can be scheduled during periods when the impact on the electricity grid is as low as possible. Energy storage systems are also becoming increasingly popular, especially for low- and medium-power consumers. The main purposes of using storage systems in optimizing the operation of distribution networks are to flatten the load curve and to store renewable energy for use at peak consumption times when hourly energy prices are high.

One of the most important goals of optimization problems is to reduce active energy losses, through the optimal use of existing control devices, as a reduction in operating costs is achieved, without requiring additional investments. It should be noted that reducing losses also contributes to limiting greenhouse gas emissions.

The first category of optimization problems focuses on the optimal programming of the operation of controllable devices in order to coordinate in an optimal way the powers generated with those that are consumed. Thus, distributed sources based on fossil fuels, electrical energy storage systems, controllable consumers and electric vehicles can be programmed. For example, during periods of low load and/or peak generation from renewable sources, the charging of as many electric vehicles as possible, the storage of energy in storage systems and the operation of certain controllable household appliances such as dishwashers or laundry machines will be scheduled.

The second category focuses on the control of reactive power in order to minimize losses by reducing its circulation through the lines and transformers in the system. Thus, the aim is to generate reactive power as close as possible to consumers, with the help of distributed sources based on both renewable and classical energy, capacitor banks and reactive power control devices based on power electronics. In this case too, a reduction in the costs of operating the distribution network is achieved without additional investments, by simply using existing resources in a coordinated and efficient way.

In the relevant literature there are a very large number of applications on the topic of optimizing the operation of electrical distribution networks and microgrids. First of all, in different studies, as in the real situation, not all types of control devices are found in the network under consideration, therefore there are a significant number of variants with different combinations of control devices. Secondly, the objectives pursued in optimization problems can be varied, so a large number of possibilities also arose from this fact. The methods of solving optimization problems are also different, both the classical methods, but especially the metaheuristic ones. Finally, by making different combinations between the available control devices, the objectives pursued and the method of solving, a significant number of scientific articles published on this topic arose.

CHAPTER 1. PHOTOVOLTAIC POWER PLANTS

1.1. Basic notions

If current electricity consumption and global population are considered, solar radiation reaching the Earth's surface could provide about 20 GW for each inhabitant at any given time. There are numerous technologies for converting solar radiation into electricity. The easiest method is to use photovoltaic panels, which perform direct conversion to direct voltage by using semiconductor materials that exhibit a photoelectric effect. The photovoltaic solution can be used at any scale, starting from residential applications to photovoltaic power plants.

1.2. Photovoltaic cells

1.2.1. Materials

The most common material used in the construction of photovoltaic cells is silicon [1]. At present, their efficiency generally reaches values of 25% under standard conditions (cell temperature: 25°C; irradiance of incident light perpendicular to the cell: 1000 W/m2; AM 1.5). In order to reduce production costs, research laboratories have developed thin-film cells, which include materials that are cheaper in terms of the manufacturing process (copper, cadmium, indium, gallium, tellurium and silicon) compared to pure silicon. According to the latest reports, their efficiency reaches up to 20.3%.

1.2.2. Electrical characterization of photovoltaic cell

Under the action of solar radiation, a direct current is generated that crosses the junction due to potential difference. The intensity of the current produced by the cell is directly proportional to the irradiance. It is observed that the intensity of the current has a large variation in relation to the irradiance, while the voltage at the terminals varies between restricted limits. Electrical charges are "collected" from the surface exposed to solar radiation by a network of thin metal fingers, which cover no more than 10% of the cell's surface. Regardless of the material they are made of, photovoltaic cells have the same behavior from an electrical point of view, so they can be characterized by the same electrical parameters therefore their performance can be compared.

1.2.3. Efficiency of photovoltaic systems

A first methodology calls for the efficiency of the conversion of light energy into alternating current electricity, denoted with ηAC. It takes into account the cumulative effects of all electrical equipment in the system, including the resistances induced by wiring harnesses and their connections.

1.2.4. Estimation of the performance of photovoltaic systems

In order to estimate the operating performance of a photovoltaic system, it is necessary to know the incident irradiance in the area and at the location angle, which implies the existence of a history of irradiance in that area. Also, during operation, numerous factors intervene that affect the performance reported under standard conditions, the most important being the

degradation over time of the photovoltaic cells, the deposits of dust and other impurities on the panels, shading and heating of the cells.

1.3. The concept of dispersed generation

Dispersed generation can be defined as the model of producing electricity with the help of small installations compared to large power plants, so that it can be connected almost anywhere in the electricity system.

1.3.1. Premises for the development of dispersed generation

Starting from the definition presented at the beginning of this chapter and analyzing the evolution of the electricity sector in the world and in Romania, it can be seen that dispersed generation is not a new concept. For several decades, both in Romania and worldwide, the production, transmission and distribution of electricity have been the components of monopolistic, vertically integrated and centrally managed energy systems. The production of electricity was provided by high-power units, thermal, hydraulic or nuclear, programmed based on the criterion of the order of merit. In such a system, control and command were carried out centrally and hierarchically.

1.3.2. Characteristics of dispersed generation

In order to define the notion of dispersed generation of electricity, in the specialized literature, one can find several statements that consider different aspects: installed power, purpose, location, energy conversion technology, environmental impact, mode of operation, owner. Dispersed electricity production has a number of advantages, the most important of which are:

1. Reducing the costs of electricity transmission and distribution (dispersed sources are closer to the consumption areas);
2. Improving some quality indicators of electricity distributed to consumers:
   a) increasing security of supply, sometimes accompanied by a reduction in the number of interruptions;
   b) improving the voltage level;
3. Diversification and rational use of primary energy sources;
4. The possibility of capitalizing on renewable forms of primary energy (wind, solar, hydraulic, biomass, etc.), having the following effects:
   a) reducing greenhouse gas emissions;
   b) environmental protection.

It provides business opportunities for investors..

1.3.3. Classification of dispersed sources

In order to understand the importance and characteristics of dispersed generation, the use of classification criteria is applied, the most important of which are:

a) depending on the type of primary energy used;
b) depending on the condition of the operation of the dispersed generation installations;
c) depending on the owners/promoters of the dispersed sources.

Depending on the type of primary energy used, dispersed sources can be classified into:

a) dispersed sources using renewable energy such as: solar, wind, hydraulic, biomass, etc.;

b) dispersed sources that run on non-renewable energy (fossil fuels): oil, natural gas, etc.

1.4. Connection diagrams of dispersed sources

The nominal voltage of the generators is established by the manufacturer, based on technical and economic considerations, and may have values belonging to the low or medium voltage range. Depending on the ratio between the nominal voltage of the generators and the nominal voltage of the electrical network, the connection can be made in two ways: a) by direct connection, if the nominal voltage of the generator coincides with that of the electrical network and b) by transformer, if the nominal voltage of the generator is lower than the nominal voltage of the electrical network.

CHAPTER 2. MICROGRIDS LOAD FLOW

A microgrid is made up of a group of consumers, distributed energy sources and/or storage systems that operate as a single controllable entity in relation to the national energy system. They can work connected to the national energy system or they can disconnect and operate in islanding mode. The concept of microgrids was introduced in the context of increasing electricity consumption and the tightening of measures to limit climate change, implemented globally. In this context, the installation of new production capacities based on renewable energy sources has become a major priority for the development of electricity systems.

In general, the following entities can be part of the structure of a microgrid: 1) consumers who can be residential, industrial and/or commercial and who can have controllable loads; 2) distributed energy sources that can be photovoltaic, wind, micro-hydropower plants or diesel or gas generator sets; 3) electricity storage systems that aim to store the energy generated in excess so that it can be used in deficit periods and 4) the energy management system that has the role of controlling all the devices within the microgrid..

2.1. Modeling of the elements of the electrical network

2.1.1. Electrical lines

The electrical lines are modeled, in the calculation of the steady state of operation, with the help of the equivalent scheme in Π. In Figure 2.1, we consider a power line connected between the nodes *i* and *k*, having the voltages $\underline{V}_i$ și $\underline{V}_k$. The equivalent scheme in Π is used for modeling both overhead power lines and power lines in cables.

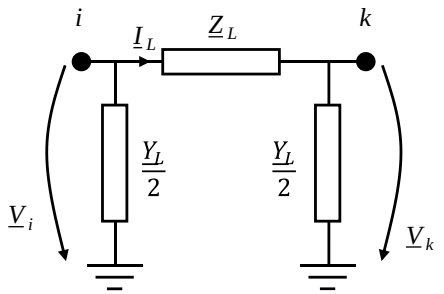

Figura 2.1. Π-equivalent scheme for modelling power lines [7].

In the equivalent scheme in Π, the power lines are modeled by means of a longitudinal impedance, $\underline{Z}_L$ and a transverse admittance $\underline{Y}_L$, and the current running through the line is denoted $\underline{I}_L$. Since the transverse admittance is divided into two equal halves placed at the ends of the line, the equivalent scheme in Π is symmetrical [7].

2.1.2. Electrical Transformers

2.1.2.1. Modeling the ideal transformer

A transformer is considered ideal if active and reactive power losses are neglected. Consequently, it is modeled by means of a transformation ratio *N*. If the transformer is provided with a tap changing mechanism, *N* is defined as the ratio of the nominal voltage of the fixed winding U_{nf} to the voltage of the adjustable winding U_{nr}, [7].

2.1.2.2. Equivalent scheme in Γ

Electrical transformers are modeled, within the calculation of the steady state mode, with the help of the equivalent scheme in Γ [7]. The equivalent Γ diagram contains the transformation ratio *N*, through which the ideal transformer is modeled, along with the longitudinal impedance $\underline{Z}_T$ and the transverse admittance $\underline{Y}_T$, through which the losses of real transformers are modeled. The equivalent scheme in Γ is not symmetrical, so it is drawn up differently for step-down transformers (Figure 2.2.a) and step-up transformers (Figure 2.2b)

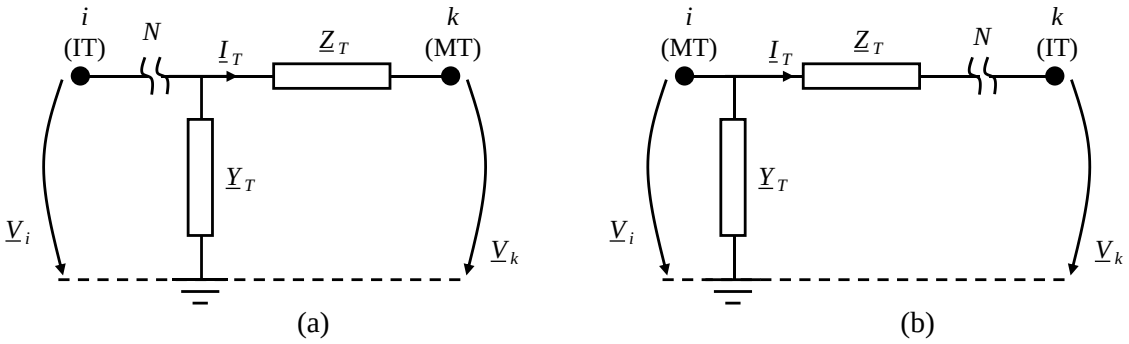

Figure 2.2. The diagram equivalent in Γ of a transformer: (a) step-down and (b) step-up [7].

2.1.3. Loads and Distributed Sources

In the steady state calculation, the loads are modeled by means of a constant apparent power, absorbed from the connection node *i*, according to [7]:

$$\underline{S}_{i,c} = P_{i,c} + jQ_{i,c} \qquad (2.1)$$

The distributed energy sources are also modeled as constant apparent powers injected at the conection node *i*, according to [7]:

$$\underline{S}_{i,g} = P_{i,g} + jQ_{i,g} \qquad (2.2)$$

Therefore, at each node *i* of the electricity grid, the active, reactive and complex apparent nodal powers P_i, Q_i and $\underline{S}_i$ are defined as the difference between the demanded $P_{i,c}$, $Q_{i,c}$ and $\underline{S}_{i,c}$ and generated powers $P_{i,g}$, $Q_{i,g}$ and $\underline{S}_{i,g}$:

$$\underline{S}_i = \underline{S}_{i,c} - \underline{S}_{i,g} = \left(P_{i,c} - P_{i,g}\right) + j\left(Q_{i,c} - Q_{i,g}\right) = P_i + jQ_i \qquad (2.3)$$

The nodal currents $\underline{I_i}$ are defined, according to [7], on the basis of the nodal powers $\underline{Si}$ and the nodal stresses $\underline{U_i}$, as follows:

$$\underline{I_i} = \left(\frac{\underline{S_i}}{\sqrt{3} \cdot \underline{U_i}}\right)^* \quad (2.4)$$

2.1.4. Capacitor Banks and Compensating Inductors

The devices for the control of the reactive power, namely the capacitor batteries and the compensating coils, are modeled as a constant admittance $\underline{Y_0}$, connected in branch to the connection node *i* [14].

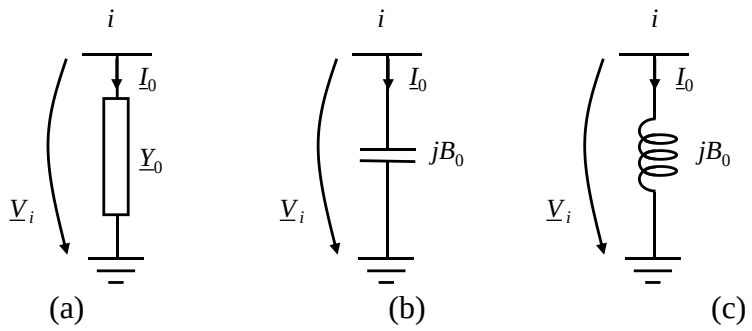

Figura 2.3. Constant admittance model of the compensating devices: (a) the general case, (b) the capacitor bank and (c) the compensating inductors [7].

2.2. Load flow calculation

2.2.1. Basics of Load flow calculation

A tree-like distribution electrical network is considered, having a number of n_N nodes, of which one is the source node (denoted 0) and the rest of $n_N - 1$ are nodes to which distributed sources and/or consumers are connected. In the mathematical model of steady state calculation, the phasors of nodal voltages and nodal currents are considered as electrical state quantities attached to the nodes, and the phasors of the currents flowing through the sides as electric state quantities attached to the sides. Of these quantities, the following are known: the voltage at the source node ($\underline{U_0} = U_{0,imp} \cdot e^{j0}$) and the active and reactive nodal powers at *the* $n_N - 1$ nodes (P_i and Q_i); and by the steady state calculation the following are determined: the voltages of the $n_N - 1$ nodes ($\underline{U_i}$) and the current circulations through the *nL* sides of the network ($\underline{I_{jk}}$).

2.2.2. Backward-Forward Sweep Method

The Backward-Forward Sweep method is a method of performing the load flow analysis, developed for electrical distribution networks, which are characterized by a radial or arborescent structure [8]. For this type of electrical networks, the Backward-Forward Sweep method has a number of advantages compared to the Newton-Raphson and Seidell-Gauss methods. According to [9], it is considered that the Backward-Forward Sweep method was introduced in 1967, in the paper [10], for the calculation of radial and unbalanced electrical networks. Since then, numerous variants [11] of the Backward-Forward Sweep method have been developed, adapted to determine the load flow of simple looped networks or to integrate distributed sources that also perform voltage regulation at the connection node.

In the present study, the Backward-Forward Sweep method is used, in which the nodal currents and the current circulations through the network branches are expressed. Thus, the load flow calculation involves an iterative process, structured in the following stages [7]:

I. Initialization;
II. Backward Sweep stage: starting from the terminal nodes and calculating the currents required by the consumers, respectively the current circulation through the sections, going to the source node;
III. Forward Sweep: start from the source node and calculate the voltage drops on the sides of the network and the voltages at the nodes, going to the terminal nodes;
IV. Performing the convergence test to determine whether to resume the upstream and downstream steps or to stop the iterative computation process.

In order to go through the backward and forward sweep stages, it is necessary to determine an order of traversal through the electrical network. In this sense, an oriented graph is created, with the same structure as that of the studied network. The graph associated with the network is traversed and determines the predecessor *Pred*(*j*) and the set of successors *Succ*(*j*) to each node *j*. Based on these, the order of traversal of the network is determined, for the descending ord_desc stage, with the help of a width traversal of the graph. Next, it is considered that any node *j* is connected with the predecessor *i* and the successors *k*, *l*, *m*. The sides connecting the vertices *i*, *j*, *k*, *l* and *m* are shown in Figure 2.4.(a), and their equivalent scheme in Figure 2.4. (b).

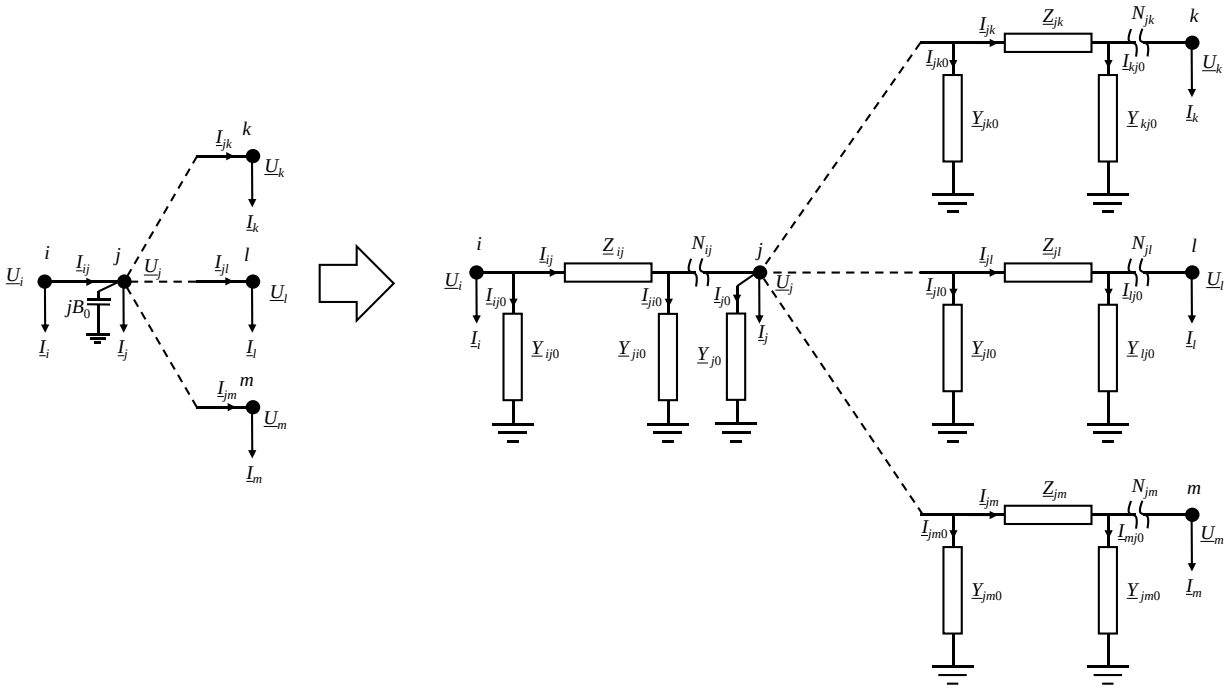

Figure 2.4. (a) The branches connecting the node *j* with the predecessor *i* and the successors *k*, *l*, *m* and (b) their equivalent scheme [14].

The algorithm of the Backward-Forward Sweep method [7] is presented below:

I. Initialization: Once the order of traversal of the electrical network has been established in the ascending *ord_asc* and descending *stages ord_desc*, the predecessor *Pred*(*j*) and the successors of each *Success*(*j*) node *j*, the iterative calculation process begins, by initializing the

counter of the iterations $p = 0$ and all unknown voltages $\underline{U}_j$ with the value of the source node voltage $\underline{U}_0 = U_{0,imp} \cdot e^{j0}$:

$$U_j^{(0)} = U_0 \, , j = 1, 2 \ldots n_N - 1 \qquad (2.5)$$

II. Backward Sweep: traverse the network from the terminal nodes to the source node and, for each node *j* and calculate [7]:

1. the current demanded by the consumer at node *j*, $\underline{I}_j$:

$$\underline{I}_j^{(p)} = \left(\frac{\underline{S}_j}{\sqrt{3} \cdot \underline{U}_j^{(p-1)}} \right)^* \qquad (2.6)$$

2. currents through the shunt admittances of the:

- power line from predecessor *i* to node *j*, $\underline{I}_{j0}$:

$$\underline{I}_{ji0}^{(p)} = \underline{Y}_{ji0} \cdot \frac{N_{ij} \cdot \underline{U}_j^{(p-1)}}{\sqrt{3}} \qquad (2.7)$$

- compensation devices connected to node *j*, $\underline{I}_{j0}$:

$$\underline{I}_{j0}^{(p)} = \underline{Y}_{j0} \cdot \frac{\underline{U}_j^{(p-1)}}{\sqrt{3}} \qquad (2.8)$$

- lines to the successors *k* of node *j*, $\underline{I}_{jk0}$:

$$\underline{I}_{jk0}^{(p)} = \underline{Y}_{jk0} \cdot \frac{\underline{U}_j^{(p-1)}}{\sqrt{3}} \qquad (2.9)$$

3. current through the power line connecting the node *j* with the predecessor *i*, $\underline{I}_{ij}$:

$$\underline{I}_{ij}^{(p)} = \frac{1}{N_{ij}} \left(\underline{I}_j^{(p)} + \underline{I}_{j0}^{(p)} + \sum_{k \epsilon Succ(j)} \underline{I}_{jk}^{(p)} + \sum_{k \epsilon Succ(j)} \underline{I}_{jk0}^{(p)} \right) + \underline{I}_{ji0}^{(p)} \qquad (2.10)$$

where: *i* is the node preceding the node *j*, *Succ*(*j*) is the set formed by the successor nodes of the node *j* and N_{ij} is the transformation ratio of the side *i* – *j*.

III. Forward Sweep: the power grid is traversed from the source node to the terminal nodes and the following are calculated [7]:

1. voltage drop on the branch connecting node *j* with its predecessor *i*, $\Delta\underline{U}_{ij}$:

$$\Delta\underline{U}_{ij}^{(p)} = \sqrt{3} \cdot \underline{Z}_{ij} \cdot \underline{I}_{ij}^{(p)} \qquad (2.11)$$

2. voltage at the node *j*, $\underline{U}_j$:

$$\underline{U}_j^{(p)} = \frac{1}{N_{ij}} \cdot \left(\underline{U}_i^{(p)} - \Delta\underline{U}_{ij}^{(p)} \right) \qquad (2.12)$$

IV. Convergence test.

1) Calculate the power output of the source at the current iteration *p*, $\underline{S}_0$ [7]

$$\underline{S}_0^{(p)} = \sqrt{3} \cdot \underline{U}_0 \cdot \left(\sum_{k \epsilon Succ(0)} \underline{I}_{0k}^{(p)} \right)^* \quad (2.13)$$

2) Determine the modulus of the difference between the value of the power output from the source at the current iteration *p* and the value from the previous iteration *p* – 1:

$$\left| \underline{S}_S^{(p)} - \underline{S}_S^{(p-1)} \right| \leq \epsilon_S \quad (2.14)$$

If the modulus of the difference is less than the permissible calculation error ε_S, the calculation stops, otherwise the iteration $p = p + 1$ is incremented and the algorithm is repeated starting with Step II.

2.2.3. Advantages of Backward-Forward Sweep Method

The Backward-Forward Sweep method has the following advantages in comparison to other load flow calculation methods, based on the Newton-Raphson and Seidel-Gauss methods, [7]:

- The computational effort is lower both for each iteration and as a total number of iterations;
- The determination of the nodal admittance matrix is not necessary, therefore the calculation time is shorter;
- Method convergence is not affected by low-impedance elements.

2.3. Load flow calculation software

2.3.1. Presentation of the calculation software

This chapter presents the calculation software for the load flow calculation of the tree distribution electrical networks, developed by the author. The software is developed by the author in the Matlab programming environment and is structured in four main modules:

M_1) Input data entry module;
M_2) Input Data Processing Module;
M_3) Load flow calculation module;
M_4) Results processing module.

The input data module M_1 consists of a template Matlab file based on which the user enters the data necessary for modeling the studied electrical network.

In module *M_2*, the input data are processed in order to form the mathematical model necessary for the application of the Backward-Forward Sweep method. In a first step, the oriented graph associated with the modeled electrical grid is constructed and the set of successors *Succ*(*j*) and the predecessor node *Pred*(*j*) is determined for each node *j*. To determine the order in which the network nodes are visited in the descending ord_desc stage, the associated graph is traversed starting with the source node, applying a width lookup strategy. The order of traversal of the vertices in the ascending stage *ord_asc* is determined by reversing *ord_desc*. Next, for each node *j* of the network, the active nodal powers P_j and reactive Q_j are determined and the admittance of the compensating devices connected in lead $\underline{Y}_{j0}$ to node *j* is calculated.

For each branch *i–k* of the power grid, the parameters of generalised schemes Π shall be calculated.

The load flow calculation module *M_3* receives as input the power grid model created by the *M_2* module and returns the load flow calculation results, i.e. nodal voltages $\underline{U}_i$, current circulations through the branches $\underline{I}_{ik}$ and power losses $\Delta\underline{S}$. The load flow calculation is performed by applying the Backward-Forward Sweep method. The flowchart of the BackwardForward Sweep is shown in Figure 2.5.

Within the *M_4* module, the user has the possibility to process the results provided by the M_3 module and generate graphs based on them.

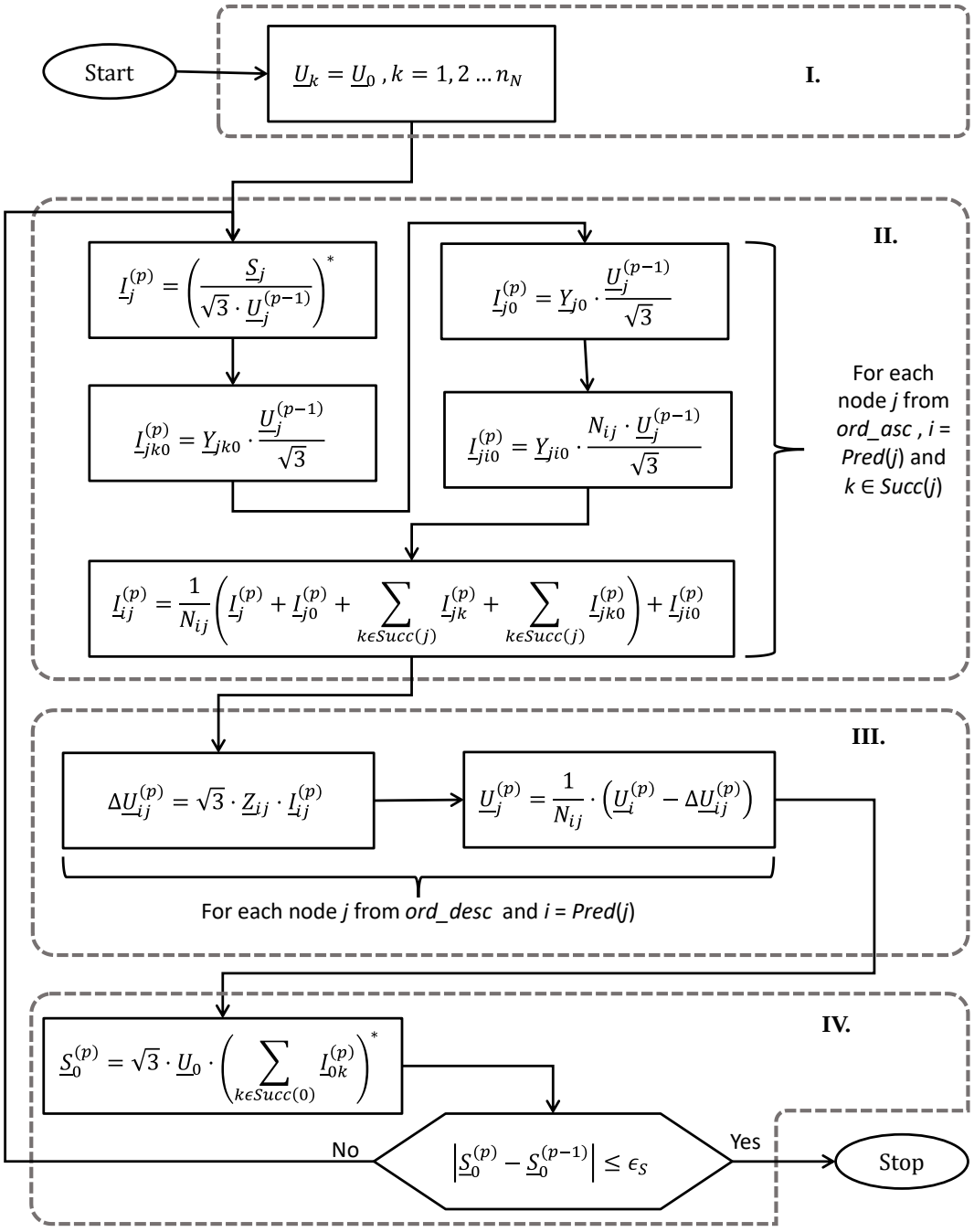

Figure 2.5. Flowchart of laod flow calculation software.

2.3.2. Validation of the calculation software

The validation of the calculation software developed by the author is achieved by comparing the results of the steady state calculation of a tree-like electrical distribution network provided by the software with those generated by a professional software, namely Neplan. For this purpose, the European MV Distribution Network Benchmark, introduced by the CIGRE association in [14], shall be considered. The results of the calculation of the load flow of the electricity grid, provided by the calculation program made by the author, are compared with those obtained with the help of the professional calculation program Neplan. Table 2.5 shows a comparison between the values of the nodal voltage obtained with the program developed by the author U_{Matlab} and those obtained with the help of the Neplan program U_{Neplan}, absolute error $\varepsilon_{abs} = U_{Matlab} - U_{Neplan}$ and relative error $\varepsilon_{rel} = \varepsilon_{abs} / U_{Neplan}$. Based on the data presented in Table 2.1, it can be seen that the errors of the program made by the author in the calculation of the nodal voltages are of maximum $8{,}5 \cdot 10^{-5}$ kV, representing $4{,}42 \cdot 10^{-8}$ %. In conclusion, the values calculated for the nodal stresses with the help of the author's program can be considered correct.

Table 2.1 Comparison of voltage levels.

Nod	U_{Neplan} [kV]	U_{Matlab} [kV]	ε_{abs} [kV]	ε_{rel} [%]
N0	110	110	0.000E+00	0.00E+00
N1	20.422	20.42192121	7.879E-05	3.86E-08
N2	19.9623	19.96221801	8.199E-05	4.11E-08
N3	19.2433	19.24327573	2.427E-05	1.26E-08
N4	19.2073	19.20721505	8.495E-05	4.42E-08
N5	19.1825	19.18249823	1.771E-06	9.23E-10
N7	19.1533	19.15326799	3.201E-05	1.67E-08
N8	19.1303	19.13022467	7.533E-05	3.94E-08
N6	19.1357	19.13562696	7.304E-05	3.82E-08
N9	19.1166	19.11654204	5.796E-05	3.03E-08
N10	19.0922	19.09220007	-6.505E-08	-3.41E-11
N11	19.0884	19.08835548	4.452E-05	2.33E-08
N12	19.9934	19.9933902	9.796E-06	4.90E-09
N13	19.8967	19.89670292	-2.925E-06	-1.47E-09
N14	19.8411	19.84108319	1.681E-05	8.47E-09

CHAPTER 3. INTEGRATION OF PHOTOVOLTAIC POWER PLANTS INTO OPTIMAL REACTIVE POWER CONTROL

3.1. Formulation of the optimization problem

3.1.1. Objective function

The purpose of this case study is to optimize the operation of a microgrid through optimal control of reactive power. To this end, the aim is to minimize the total losses of active power by controlling the reactive power generated by all existing control devices in the microgrid, both capacitor banks and photovoltaic plants. The objective function $f(x)$ is presented in relation (3.1) and implies the minimization of total losses at the network level, in the context of the application of the equality constraint set $g(x)$ and inequality $h(x)$ [25]..

$$f(x) = \min \Delta P_{tot}$$
$$\text{Subject to:} \quad g(x) = 0 \qquad (3.1)$$
$$h(x) \leq 0$$

In relation (3.1), x is the vector of the control variables x and has the following structure:

$$x = [Q_{g,1}, Q_{g,2}, \dots, Q_{g,N_{CEF}}, n_{BC,1}, n_{BC,2}, \dots, n_{BC,n_{BC}}] \qquad (3.2)$$

where $Q_{g,1}$ ... $Q_{g,NCEF}$ represents the reactive power generated by the N_{CEF} photovoltaic plants in the studied microgrid, and the operating steps of the n_{BC} capacitors banks are noted $n_{BC,1}$ ... $n_{BC,nCB}$.

The total power losses ΔP_{tot} are determined on the basis of the active power balance at the level of the entire microgrid, as the difference between the active power received by the microgrid from the slack bus P_{NE} and from the N_{CEF} PV power plants P_g and the power required by the loads P_c connected to the N nodes of the microgrid.

$$\Delta P_{tot} = P_{NE} + \sum_{i=1}^{N_{CEF}} P_{G,i} + \sum_{i=1}^{N} P_{c,i} \qquad (3.3)$$

3.1.2. Equality and inequality constraints

The equality constraints g(x) in relation (3.1) have the role of ensuring the realization of the load flow calculation for the studied microgrid [16] . For this purpose, the set of equality constraints consist of the two equations of the nodal active and reactive powers of each node i, presented in relation (3.4) [7]:

$$P_i - \sum_{k=1}^{N} U_i U_k [G_{ik} \cos(\theta_i - \theta_k) + B_{ik} \sin(\theta_i - \theta_k)] = 0$$
$$Q_i + \sum_{k=1}^{N} U_i U_k [B_{ik} \cos(\theta_i - \theta_k) - G_{ik} \sin(\theta_i - \theta_k)] = 0 \qquad (3.4)$$

where P_i and Q_i are the active and reactive nodal powers at node i, U_i, U_k, and θ_i, θ_k represent the modules and arguments of the voltages at nodes i and k, and G_{ik} and B_{ik} are the real and imaginary parts of the term $\underline{Y}_{ik}$ in the nodal admittance matrix.

The h(x) inequality constraints in relation (3.1) are implemented in order to ensure compliance with the operational limits of the controlled devices, respectively of the microgrid [16]. For capacitor banks and photovoltaic power plants, the inequality restrictions are presented in the relationship (3.5):

$$Q_{g,i}^{min} \leq Q_{g,i} \leq Q_{g,i}^{max}, \forall\, i = 1 \dots N_{PVPP}$$
$$n_{CB,i}^{min} \leq n_{CB,i} \leq n_{CB,i}^{max}, \forall\, i = 1 \dots n_{CB} \qquad (3.5)$$

where $Q_{g,i}^{min}$ și $Q_{g,i}^{max}$ are the lower and upper limits of the reactive power that can be generated by each photovoltaic plant, and $n_{BC,i}^{min}$ and $n_{BC,i}^{max}$ represents the minimum and maximum levels of each capacitor bank.

The set of inequality restrictions $h(x)$ relating to the operation of the microgrid are intended to ensure compliance with the permissible band of nodal voltages and the permissible currents of the branches [16], according to the expression (3.6):

$$\begin{gathered} U_i^{min} \leq U_i \leq U_i^{max}, \text{pentru } i = 1 \dots N \\ \left|\underline{I}_j\right| \leq I_i^{max}, \text{pentru } i = 1 \dots N_{EL} \end{gathered} \quad (3.6)$$

where U_i^{min} and U_i^{max} represents the permissible voltage limits at node i, and I_i^{max} is the allowable current through each of the N_{EL} power lines of the microgrid.

3.1.3. Model adaptations for metaheuristic algorithms

In the present paper, the solution of the optimization problem formulated in this chapter is achieved with the help of a metaheuristic algorithm. it is necessary to introduce certain adaptations of the mathematical model in order to ensure compliance with the restrictions of equality and inequality.

First, equality restrictions are applied within classical optimization methods to perform steady-state calculation. In the case of metaheuristic algorithms, this is not possible, the steady state calculation being performed within the objective function, by applying the backwardforward sweep method, thus ensuring the fulfillment of the equality restrictions presented in the expressions (3.4).

In the case of inequality restrictions on the operational limits of control devices, expressed in expressions (3.5), it is not necessary to introduce additional adaptations, as these restrictions are integrated into metaheuristic algorithms as lower and upper limits of control variables Q_g and n_{CB}. However, in order to comply with the restrictions regarding the operational limits of the microgrid, in the expressions (3.6), it is necessary to introduce penalty functions, with the role of increasing the value of the objective function for individuals who do not comply with the inequality restrictions. In order to apply the penalty functions, it is necessary to replace the objective function $f(x)$ with the penalized objective function $F(x)$, defined on the basis of which the two penalty functions P_1 and P_2 and a coefficient α are added, [16]:

$$F(x) = f(x) + \alpha + P_1 + P_2 \quad (3.7)$$

During the optimization process, individuals may appear for whom the steady state calculation does not converge. A penalty must be applied to these individuals, α, as high as possible in order to quickly eliminate them from the population. The first inequality restriction related to the operational limits of the microgrid in expressions (3.6) refers to the framing of nodal voltages within the permissible range $[U_i^{min}, U_i^{max}]$. In order to ensure compliance with this restriction, the penalty function *P1* shall be defined, which shall be calculated as the sum of the penalty coefficients $p_{1,i}$ related to each node of the microgrid, multiplied by a coefficient C_1 which aims to scale the numerical values in a favorable way.

$$P_1 = C_1 \sum_{i=1}^{N} p_{1,i} \quad (3.8)$$

For each node of the microgrid, the penalty coefficient $p_{1,i}$ is equal to zero, if the nodal voltage falls within the permissible limits. In case of exceeding the upper limit of the voltage, the coefficient is equal to the difference between the value of the voltage and its maximum permissible value, and in case of exceeding the lower limit, to the difference between the minimum permissible voltage and the nodal voltage.

$$p_{1,i} = \begin{cases} (U_i^{min} - U_i)\ if\ U_i < U_i^{min} \\ 0 \quad if\ U_i^{min} \le U_i < U_i^{max} \\ (U_i - U_i^{max})\ if\ U_i > U_i^{max} \end{cases} \quad (3.9)$$

The second inequality constraint in terms of microgrid boundaries relates to compliance with the maximum allowable currents through the microgrid sides. To this end, the penalty function P_2 shall be introduced within the penalised objective function F. The latter is determined as the sum of the penalty coefficients $p_{2,i}$ for each power line in the microgrid, multiplied by a coefficient C_2, in order to scale the numerical values in a convenient way.

$$P_2 = C_2 \sum_{i=1}^{N_{LE}} p_{2,i} \quad (3.10)$$

For each electric line within the microgrid, the value of the penalty coefficient $p_{2,i}$ shall be determined as the difference between the current through the line and the maximum permissible current, if this restriction is not complied with, or zero otherwise.

$$p_{2,i} = \begin{cases} 0 \quad if\ |\underline{I}_i| \le I_i^{max} \\ (|\underline{I}_i| - I_i^{max})\ if\ |\underline{I}_i| > I_i^{max} \end{cases} \quad (3.11)$$

3.2. Metaheuristic optimization algorithms

3.2.1. General terms

Metaheuristic algorithms are procedures for finding the optimal solution in the solution space, which usually rely on mimicking natural processes to solve optimization problems. The name metaheuristic comes from the term heuristic which involves finding the solution with the help of a set of rules based on experience, to which is added the prefix meta which shows that these rules can be applied in different fields, they are considered generally valid principles not being specific to a certain set of problems. Unlike classical optimization methods, metaheuristic algorithms do not have a mathematical model for minimizing the objective function, based on mathematical theorems, applying a set of rules inspired by nature to guide the search process towards the best solution.

The mechanism of operation of metaheuristic algorithms is in principle presented below. It starts from one or more candidate solutions, usually chosen randomly. The value of the objective function for each of the candidate solutions is then determined and based on its value, the performance of each solution is evaluated. The process by which a new set of candidate solutions is determined is very different from one algorithm to another, but usually, new solutions are guided according to the positions of the best performing solutions existing in the current iteration. Within the search process, two main stages are distinguished, namely: exploration – when the solutions are scattered to cover the space of the solutions as best as possible – and exploitation – when the solutions converge on the area where the algorithm has identified the best solutions.

3.2.2. Grey Wolf Optimizer

The Grey Wolf Optimizer (GWO) algorithm was introduced by S. Mirjalilil in 2014, inspired by the social behavior of grey wolves (Canis lupus), which hunt in packs and use cooperation and coordination to find prey [17]. Within the pack, wolves have a very welldefined

hierarchy of social dominance. The social structure of a wolf pack comprises four categories of individuals, hereinafter referred to as alpha, beta delta, and omega. The alpha wolf is the one who leads the pack, being assisted in decision-making and in the management of the pack's activities by beta and delta wolves. The rest of the wolves in the population are called omegas and are subordinate to the three dominant types of wolves.

Within the grey wolf algorithm, the three categories of dominant wolves, alpha, beta, and delta are modeled separately from the rest of the pack by selecting the three top-performing wolves discovered so far in the current iteration. The position of each wolf in the pack is updated based on the positions of the three dominant wolves with the help of the relationship [17]:

$$X = \frac{X_1 + X_2 + X_3}{3} \quad (3.12)$$

Variables X_1, X_2 and X_3 are the positions that the current wolf X would take according to each type of alpha, beta and delta dominant wolf and are calculated with the relationships [28]:

$$\begin{aligned} X_1 &= X_\alpha - A_1 \cdot |C_1 \cdot X_\alpha - X| \\ X_2 &= X_\beta - A_2 \cdot |C_2 \cdot X_\beta - X| \\ X_3 &= X_\delta - A_3 \cdot |C_3 \cdot X_\delta - X| \end{aligned} \quad (3.13)$$

In relations (3.13) the positions of alpha, beta and delta dominant wolves are denoted with X_α, X_β și X_δ., and the terms A_1, A_2 și A_3 and C_1, C_2 și C_3 are calculated based on random numbers r_1 și r_2 with values in the range [0,1] using the following expressions [17]:

$$\begin{aligned} A &= 2 \cdot a \cdot r_1 - a \\ C &= 2 \cdot r_2 \end{aligned} \quad (3.14)$$

Terms A_1, A_2 și A_3 have the role of ensuring the balance between exploration and exploitation processes. Thus, the term decreased linearly from 2 to 0 during the iterations, and for values of $a > 1$ wolves tend to scatter, moving away from the dominant wolves in order to explore the space of solutions as best as possible. In the case of $a < 1$ values, the wolves converge on the positions of the dominant wolves, thus ensuring the efficiency of the exploitation process. Coefficients C_1, C_2 și C_3 have the role of ensuring a weighting of the influence of the position of the dominant wolves α, β and δ in the future position of the current wolf.

3.2.3. Genetic algorithms

Genetic algorithms belong to the category of metaheuristic algorithms and are based on Charles Darwin's theory of the evolution of species in nature. Genetic algorithms were introduced by John Holland, professor of computer science at the University of Michigan, in the 1960s, and the reference publication for this field "Adaptation in Natural and Artificial Systems" was published in 1975 by the same J. Holland [20]. Thus, the foundations of the new scientific field, metaheuristic algorithms, were laid. In genetic algorithms, each potential solution is modeled as an individual that is part of a population. The operating principle of genetic algorithms consists in the improvement of individuals within the population, over several generations, with the help of three mechanisms inspired by the evolution of species in nature, namely selection, crossover and mutation [20].

3.2.4. Particle Swarm Optimization

Particle Swarm Optimization - PSO is a metaheuristic optimization algorithm, introduced in 1995 by James Kennedy and Russell Eberhart [21]. Due to the very good performance obtained with the help of a relatively simple mathematical model, PSO has become very popular in the scientific literature, gathering, at the time of writing this paper, a number of over 87000 citations, according to the Google Scholar platform. The inspiration for this algorithm lies in the social behavior of flocks of birds or schools of fish. Thus, for each individual in the population, two different components are considered that influence the direction of travel. The cognitive component is based on their own experience, with each individual memorizing the best position determined up to the current iteration. The social component is based on the experience of the whole group and has the effect of guiding individuals towards the best position determined at the level of the entire population until the current iteration [21].

3.2.5. Sine-Cosine Algorithm

Sine-Cosine Algorithm (SCA) is a relatively recent metaheuristic algorithm, proposed by S. Mirjalili in 2016,[23] which is based on oscillations generated by the two trigonometric functions sine and cosine. SCA is a popular metaheuristic algorithm, being used in solving a significant number of optimization problems, due to the very simple mathematical model, based on which good performance is obtained [24].

3.2.6. Salp Swarm Algorithm

Salp Swarm The algorithm is inspired by the behavior of salps and was proposed by S. Mirjalili in [26]. Salpias are part of the Salpidae family, but are visually similar to jellyfish and have a swarm-like behavior when feeding in a spiral.

3.3. Case study

3.3.1. Microgrid studied

The case study presented in this subchapter is carried out on a microgrid with a nominal voltage of 20 kV, which supplies seven consumers through seven underground MV power lines, from the MV bars of a step-down transformer. Within it, four photovoltaic power plants are connected to nodes 2, 3, 6 and 8 and three capacitor banks at nodes 4, 5 and 7. The single-line diagram of the microgrid, inspired by the European version of the CIGRE MV reference network [14], is shown in Figure 3.1.

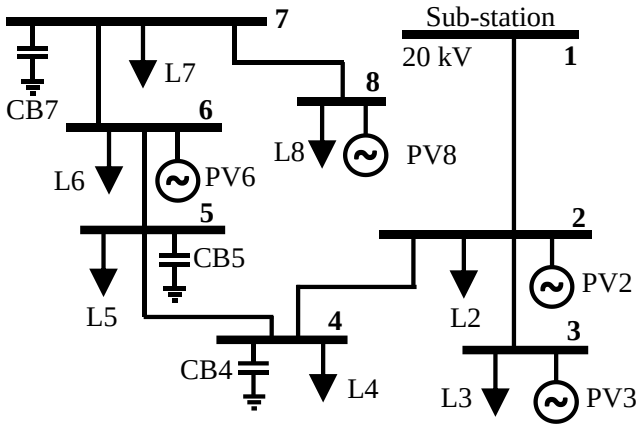

Figure 3.1. The microgrid studied [27].

The simulations presented in this case study are performed on several scenarios by solving the optimization problem formulated in chapter 3.1 using the Gray Wolf Optimizer presented in chapter 3.2.1. All simulations are performed in the Matlab environment, based on the software codes created by the author to solve the optimization problem, perform the load flow calculation of the microgrid using the backward-forward sweep algorithm and data processing. It is noted that the GWO code used in this work is the one provided by S. Mirjalili, available online on his personal website.

3.3.2. Comparison of metaheuristic algorithms

The reactive power management optimization problem presented in chapter 3.1 is solved by using five different metaheuristic algorithms, namely: Grey Wolf Optimizer (GWO), Salp Swarm Algorithm, Particle Swarm Optimization (PSO), Sine-Cosinus Algorithm (SCA) and Genetic Algorithm (GA). The population size of 100 individuals and the maximum number of iterations of 100 are imposed for all algorithms to obtain a coherent comparison of performances, while for the other parameters within each metaheuristic algorithm the default values from the literature are used. Also, 50 consecutive runs were performed for each algorithm considered in order to obtain a relevant set of runs for the analysis of their performance in solving the optimization problem [29].

Figure 3.2 shows the minimum, average and maximum values obtained by the five algorithms in the 50 simulations carried out for each. Based on the figure, it follows that all algorithms obtain at least one solution with objective function value below the threshold of *fobj* = 0.92024 r.u., while GWO and SSA obtain the best minimum value of 0.91997 r.u., followed by PSO with 0.9199 r.u., GA with 0.92 r.u., and SCA again obtains the lowest value of 0.9204 r.u. In terms of average values, GWO gets the best value, while PSO ranks second and SSA ranks third, followed by GA and SCA. Also, the Grey Wolf Optimizer (GWO) achieves the best performance in terms of the maximum value determined in the 50 runs.

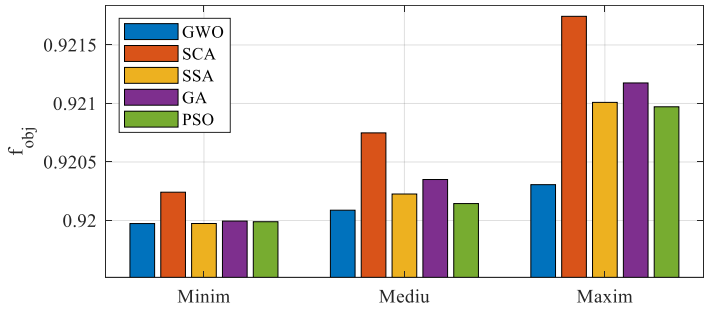

Figure 3.2. The minimum, average and maximum values obtained by the algorithms considered in the 50 runs.

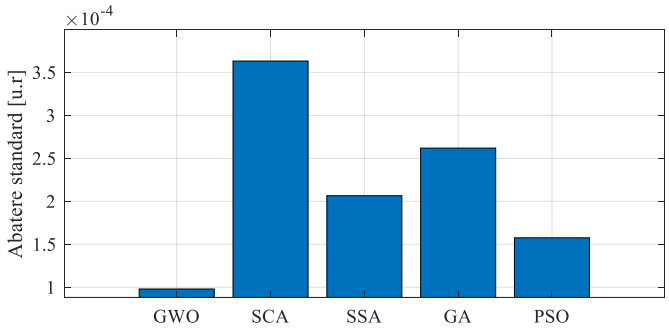

Figure 3.3. Standard deviation for the solutions obtained by the considered algorithms.

The standard deviation for the solutions provided by the five algorithms considered in the 50 successive runs is shown in Figure 3.3. The results show that GWO determines the most consistent results, with a standard deviation of $9.8 \cdot 10^{-5}$ r.u. in the 50 successive runs, followed by the PSO with a standard deviation of $1.58 \cdot 10^{-4}$ r.u. If in the case of the minimum and average values obtained by GWO and PSO the differences are relatively small, in the case of standard deviation, the value obtained by GWO is 1.6 times lower than in the case of PSO, indicating that GWO is clearly superior to the other algorithms in terms of consistency.

3.3.3. Integrating PVPP into reactive power control

In this analysis, three different scenarios of the power demanded by consumers are considered, namely at the off-peak load (S1), base load (S2) and peak load (S3). The baseline load scenario is defined by the initial consumption values. The off-peak load scenario is defined by reducing the required active and reactive power by 15% for all consumers, while the peak load scenario is characterized by a 15% increase in required power. Also, five other scenarios are defined for the power generated by the PVPP, considering the power generated by the plants, P_{PVPP}, at 0%, 25%, 50%, 75% and 100% of the nominal active power P_{max}. A total of 15 scenarios will be obtained by generating all possible combinations between the three consumption scenarios and the five power plant scenarios [27] shown in Table 3.1.

Table 3.1. Considered scenarios

P_{CEF} (%) / Scenario	0%	25%	50%	75%	100%
Load Gap	S.1.0	S.1.1	S.1.2	S.1.3	S.1.4
Base Load	S.2.0	S.2.1	S.2.2	S.2.3	S.2.4
Peak load	S.3.0	S.3.1	S.3.2	S.3.3	S.3.4

The case study presents the impact of the integration of photovoltaic power plants in the reactive power control, on the active power losses of the microgrid and the voltage profile, for the 15 scenarios considered. For each scenario, a reference strategy is defined in which the control of the reactive power is carried out exclusively through capacitor banks, while the photovoltaic power plants operate at unity power factor. Also, the impact of the reactive power generated by photovoltaic power plants on the operating conditions of the microgrid is easier to highlight compared to the reference strategy, where the optimal operating steps of capacitor banks is determined by solving a simplified version of the optimization problem formulated in chapter 3.1, in which there are only the variables $x_{CB,1}, \ldots x_{CB,n}$.

Figure 3.5 shows the optimal values obtained by the grey wolf algorithm for the reactive power generated by the four photovoltaic power plants in each of the 15 scenarios considered, and the values obtained for the operating steps of the three capacitor banks are presented in Figure 3.4.

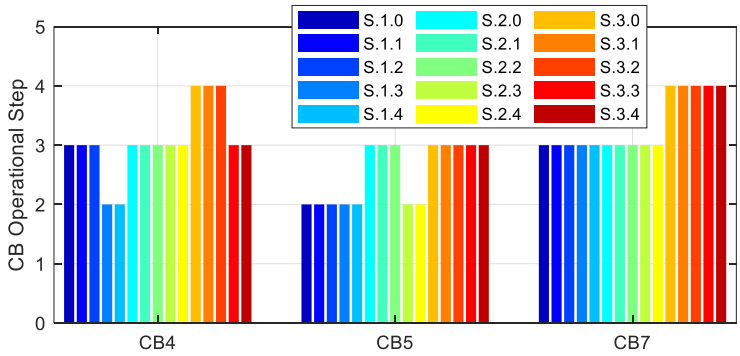

Figure 3.4. Optimal values for capacitor banks operating steps.

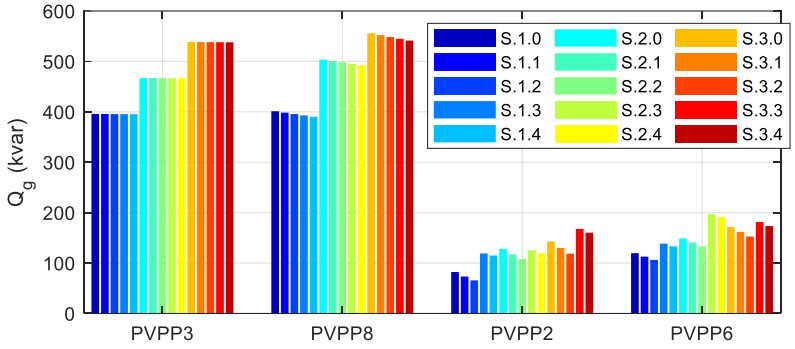

Figure 3.5. The optimal values of the reactive power generated by the four PVPPs.

From Figure 3.4 it can be seen that within the same type of scenario, the values of the operating steps of capacitor banks are constant or vary by no more than one unit. For example, in off-peak load scans (S.1), CB5 and CB7 operate on the same step 2 and 3, respectively, and CB4 operates on step 3 in scenarios S.1.0 – S.1.2 and on step 2 in scenarios S.1.3 and S.1.4. In the case of baseload scenarios (S.2), CB4 and CB7 operate on step 3, while CB5 is set on step 3 in scenarios S.2.0 to S.2.2, and then on step 2 in scenarios S.2.3 and S.2.4. The behavior of capacitor banks is explained firstly by the fact that each step has 100 kVAr, a relatively high value so that the optimization algorithm has only a rough adjustment, secondly by the change in power required by consumers. Also, from Figure 3.5, it can be seen that the reactive power output of PVPP3 and PVPP8 shows a slight decrease when increasing the active power generated. The decrease in the reactive power when the active power generated increases can also be observed in the case of the other two power plants, PVPP2 and PVPP6, with the mention that this takes over the differences in reactive power generated by the change in the operating steps of the capacitor banks.

Figure 3.6 shows the minimum (*Umin*) and average (*Uavg*) values of nodal voltage for both baseline and optimal strategies in all 15 scenarios considered. The lowest values of the minimum voltages are obtained in the S.3.0 scenario when the peak load coincides with the shutdown of the photovoltaic plants. In this case, an increase in *Umin* values is observed from 0.950 r.u. in the reference strategy to 0.952 r.u. in the optimal strategy. As expected, the impact of the reactive power generated by the PVPP on the voltage profile of the microgrid is low, as the reactive power injected by CB into the baseline strategy of approximately 1500 kVAr, is replaced by a total reactive power between 1700 kVAr (at no-load) and 2500 kVAr (in peak load scenarios) injected by both PVPPs and CB.

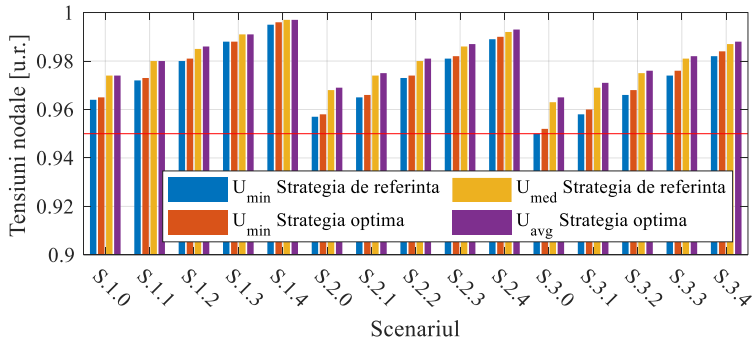

Figure 3.6. Comparison between the minimum and average bus voltages U_{min} and U_{med}.

The reduction in active power losses is shown in Figure 3.7, expressed as a percentage of the baseline. The blue bars represent the off-peak load scenarios, the basic scenarios are

represented by the red bars, and the peak load by the yellow bars. The bars are grouped in the figure by the active power generated by the *PVPPs* (P_{PVPP}), expressed as a percentage of the rated active power P_{max}.

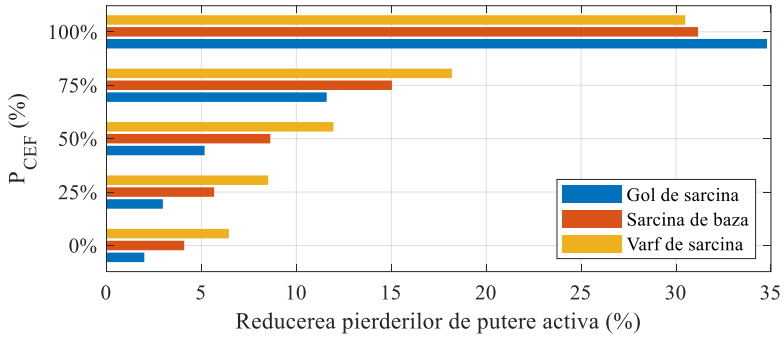

Figure 3.7. Reduction of active power losses.

The results presented in Figure 3.7 show a considerable reduction in active power losses of up to 34.8%, due to both the continuous control of the reactive power generated by the PVPPs compared to the stepwise variation of the reactive power output of the CB and a better distribution of the reactive power sources in the microgrid.

CHAPTER 4. OPTIMAL REACTIVE POWER CONTROL EXCLUSIVELY BASED ON PHOTOVOLTAIC POWER PLANTS

4.1. Strategies for PVPP reactive power control

Reactive power control is of particular importance in the operation of power grids in general, as it can bring significant advantages without requiring major investments in the installation of new devices [30]. The concept of microgrid has a major advantage over classic electricity distribution networks in that it represents a group of interconnected resources, which naturally have convergent interests and objectives, with the possibility of integrating all devices into a centralized control.

4.1.1. Constant power factor

In the first stage of the integration of renewable energy sources, most distribution and transmission system operators required photovoltaic plants to operate at a unity power factor [32], therefore they could not participate in any way in the regulation of reactive power [33]. As the development of new renewable generation capacities has become one of the main objectives of the development of power systems, the requirements for the integration of distributed sources have been revised. Currently, grid operators have made it mandatory for photovoltaic plants to operate at any power factor within a specified range [$\cos\varphi_{min}$, $\cos\varphi_{max}$] for any active power output.

4.1.2. Local compensation of reactive power

In the specialized literature, different strategies for controlling the reactive power have been proposed and analyzed, among which the compensation of the local consumer is mentioned [35]. Under this strategy, renewables are considered to be connected to nodes from which they are powered and consumers. The objective pursued is to ensure, in a certain proportion or totally, the reactive power required by consumers by the source distributed from their connection node [35].

In this control strategy, the reactive power limits of distributed sources must also be considered Q_{min} and Q_{max}, so that the reactive power generated by each source will be calculated with the relationship:

$$Q_g = \begin{cases} Q_c \ if \ Q_c \leq Q_{max} \\ Q_{max} \ if \ Q_c > Q_{max} \end{cases} \quad (4.1)$$

If the reactive power limits are calculated according to a minimum and maximum power factor, their values shall be directly proportional to the active power supplied by the source. In order to eliminate this limitation, the use of extended reactive power limits has been proposed in the literature [36]. In the case of photovoltaic power plants, the reactive power limits Q_{min} and Q_{max}, corresponding to the maximum power factor and calculated at the maximum generated active power, can also be ensured at partial active powers up to close to zero. Thus, it is possible to compensate for the reactive power required by local consumers for longer periods of time. Figure 4.1 shows a comparison of the reactive power that can be generated in the case of the application of the regular (a) and extended (b) reactive power limits.

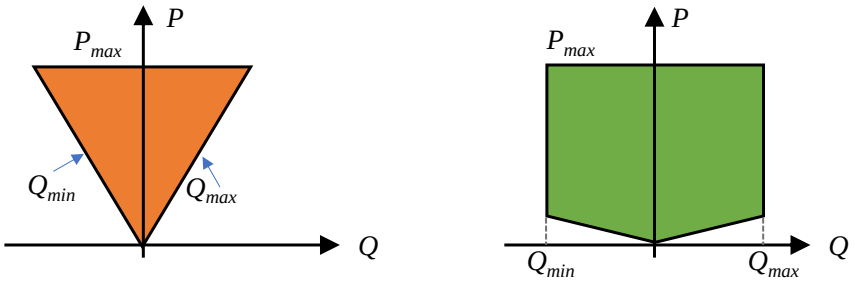

Figure 4.1. Reactive power limits for PVPPs [34].

4.1.3. Optimal reactive power control

The second version of the optimization problem aims to minimize active power losses, by achieving optimal control of reactive power within microgrids, exclusively with the help of distributed sources. The objective function f_{obj} for this version of the optimization problem is identical to the one presented in chapter 3.1.1 and consists of the total losses of active power in the microgrid, which must be minimized respecting the restrictions of equality g(x) and inequality h(x) [37]:

$$\begin{aligned} \min f(x) &= \Delta P_{total} \\ g(x) &= 0 \\ h(x) &\leq 0 \end{aligned} \quad (4.2)$$

The vector of the control variables x, in this case contains only the reactive powers generated by each of the N_{SD} distributed sources, denoted $Q_{g,i}$.

$$x = [Q_{g,1}, Q_{g,2}, \dots, Q_{g,i}, \dots, Q_{g,N_{SD}}] \quad (4.3)$$

The set of equality constraints $g(x)$ in relations (4.2) consists of the nodal power equations and are identical to those presented in relations (3.4) in chapter 3.1.2. While the set of inequality constraints $h(x)$ of the same relations (4.2) contains the restriction on the reactive power limits of the distributed sources involved in the optimal control, presented in relation (3.5) of Chapter 3.1.2, and the two restrictions on the framing of nodal voltages and lateral currents within the permissible limits, presented in relations (3.6) of the same Chapter 3.1.2.

In this case study, two versions are considered for determining the reactive power limits of distributed sources, both based on the maximum and minimum values of the power factor $\cos \varphi_i^{min}$ and $\cos \varphi_i^{max}$. In the first version, the usual limits for reactive powers determined according to the power generated and the limits of the power factor are considered.

$$Q_{g,i}^{min} = P_{g,i} \cdot \tan\left(\operatorname{acos}\left(\cos \varphi_i^{min}\right)\right) \quad (4.4)$$

$$Q_{g,i}^{max} = P_{g,i} \cdot \tan(\operatorname{acos}(\cos \varphi_i^{max})) \quad (4.5)$$

In the particular case of renewable sources and especially photovoltaic ones, the powers generated are close to the nominal power only at lunchtime, being relatively low during the morning and evening. For this reason, the literature proposes the use of extended limits for reactive powers. For this purpose, the minimum and maximum limits of the reactive powers shall be determined according to the limit values of the power factor applied to the rated active power P_{max} not to the generated power. From a technical point of view, inverters can operate with extended reactive power limits, in normal operation without the need for additional measures and without the need for higher wear. Only one limitation is introduced when operating with very low power, on the order of 10% of , when the reactive power limits decrease linearly to zero as the active power decreases to zero. For this reason, the reactive power that can be provided by the inverters is within the range $[Q_g{}^{min}{}_{,i}, Q_g{}^{max}{}_{,i}]$ for values of active power generated higher than the minimum power from which the capacity of inverters to provide reactive power is reduced $P_g{}^{min}{}_{,i}$ and zero for the rest.

$$Q_{g,i}^{min} = \begin{cases} P_{g,max} \cdot \tan\left(\operatorname{acos}\left(\cos \varphi_i^{min}\right)\right) \text{ pentru } P_{g,i}^{min} \leq P_{g,i} \leq P_{g,i}^{max} \\ 0, \quad \text{otherwise} \end{cases} \quad (4.6)$$

In order to adapt the mathematical model to the metaheuristic algorithms, we proceed in a similar way to the previous optimization problem, by implementing the objectively penalized function.

4.2. Studied microgrid

The microgrid considered in this case study, supplies nine different consumers, as follows: a hotel, an office building, a school, a shopping mall, a hospital and four residential areas. Also, five photovoltaic power plants (PVPPs) are installed in this microgrid. The microgrid consists of seven underground medium-voltage power lines and is powered by the 20 kV busbars of a downstream power station. Figure 4.2 shows the arborescent topology of the studied microgrid, which is inspired by the CIGRE MT reference network described in [14].

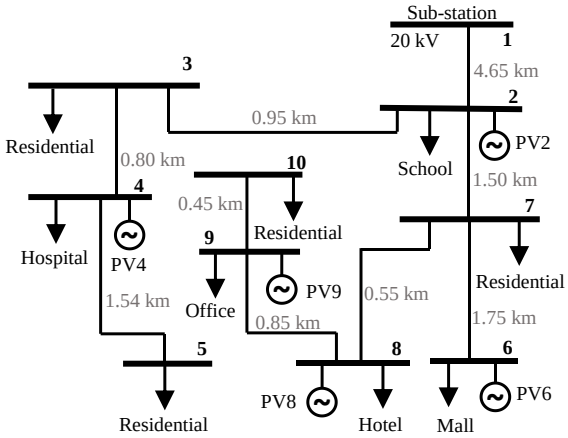

Figure 4.2. Single line diagram of the studied microgrid [37].

The load profiles are defined for each type of load, therefore, the same relative variation will be recorded for two loads of the same type, the difference being given by the maximum powers required by each load. The active powers generated by the PVPP are obtained from the Renewables Ninja database [39]. From this database, the hourly average values of the active powers generated during an entire calendar year are obtained, expressed as percentages in relation to the nominal power *Pmax*. In the study, an identical production curve is considered for the five PVPPs, due to their location in a relatively small geographical area. The percentage values are identical for each hour of the year, but they are expressed relative to the nominal power of each plant: 350 kW, 970 kW, 550 kW, respectively 1150 kW.

4.3. Analysis of the operation of the microgrid

4.3.1. 16th of May

The first analysis of the functioning of the microgrid during a day, presented in this study, refers to May 16. This day was selected because it is a combination of high values of both the power demanded by consumers and the power generated by photovoltaic plants. The selected day is among the top 5% days with the highest power generated by photovoltaic power plants and in the top 10% in terms of consumption. The load curves for each type of consumer and the production curves, both expressed as percentages, are shown in Figure 4.3.

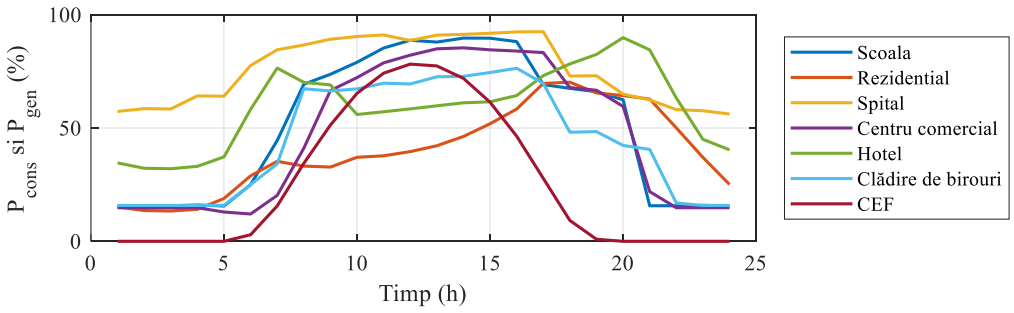

Figure 4.3. Load and production curves, expressed in percentages, for 16th of May.

The operation of the microgrid was simulated for each time slot, on May 16, in case of applying each of the 8 strategies for controlling the reactive power considered. Strategy A consists of operating the PVPP at a unity power factor, in strategies B1, B2 and B3 PVPPs operates at a constant power factor cosφ of 0.95, 0.90, respectively 0.85, while in strategies C, photovoltaic plants operate with the purpose of compensating the local load, and in strategies

D, the reactive power output by the PVPPs is determined with the aim of minimizing active power losses at the level of the entire microgrid. The difference between strategies C1 and C2, respectively D1 and D2 lies in the choice of reactive power limits. Thus, in cases C1 and D1 the limits are chosen according to the maximum power factor applied to the power generated, while the reactive power limits of the PVPPs are extended in cases C2 and D2, by applying the maximum power factor to the rated power, regardless of the active power generated. The reactive power generated by each PV plant, for each strategy, is shown in Figures 4.4 (a) – (e).

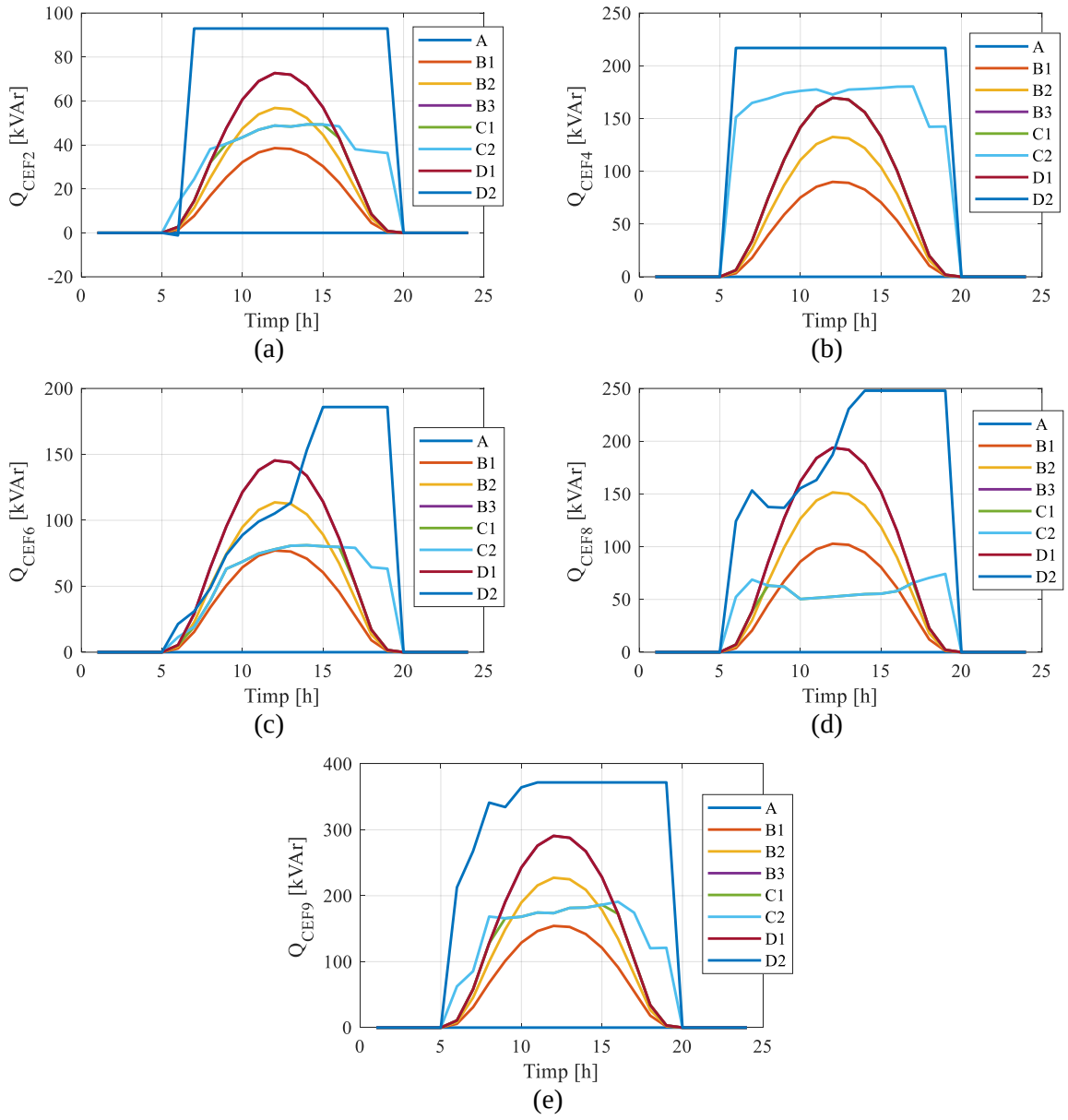

Figure 4.4. The reactive powers generated by the CEF, on May 16th , for the 8 considered strategies.

For the five plants connected to the microgrid considered, it can be seen that in the case of control strategies with constant power factor, B1, B2 and B3, the reactive power output is proportional to the active power generated. In the case of strategy C1, the conventional limits of reactive power determined by the B3 curve shall be considered, as it corresponds to the maximum power factor of 0,85. In the case of PVPP2, PVPP6, PVPP8 and PVPP9, the two curves C1 and B3 are superimposed, until 7 or 8 o'clock, and then the reactive power generated in the C1 strategy is lower than the B3 limit, as the reactive powers required by school, shopping mall, office building and hotel consumers are lower. On the other hand, in the case of the power

plant connected to node 4, where the hospital-type consumer is connected, the reactive power generated in the C1 strategy is equal throughout the day to its maximum limit. Within the C2 strategy, it can be seen that each plant manages to generate enough reactive power to compensate for the reactive power required by the local consumer.

Within the D1 and D2 strategies, the reactive powers generated by the PVPP are optimized in order to minimize the losses of active power at the microgrid level. The reactive power generated by PVPP2 and PVPP4 is at the upper limit in the D2 strategy throughout the day. In the case of the other PVPP6, PVPP8 and PVPP9 plants, the reactive power is equal to the upper limit, only for a certain part of the day. The extended reactive power limits are used by three plants, PVPP2, PVPP4 and PVPP9, throughout the day, and by PVPP6 and PVPP8 for 6 and 13 hours, respectively. For this reason, the D1 curves are superimposed either on the D2 curves, when the reactive power falls within the conventional limits, or on the B3 curves, when the upper limit is exceeded.

Figures 4.5 (a) and (b) show the profiles of the minimum and average nodal voltages recorded in the microgrid during the 24 hours in the case of the application of the eight strategies. The results presented in Figures 4.5 (a) and (b) show that the best minimum and average voltage levels are observed when the PVPP operates according to the optimal control strategy with extended limits D2 and local compensation with extended limits C2. Also, the voltage level decreases as the power factor increases, and strategy A, characterized by cosφ = 1, registers the lowest voltage values. It can be seen that the voltage level improves as the reactive power injected by the PVPPs increases, therefore the best voltage values are recorded in the optimal control strategy with extended limits D2. On the other hand, the influence of the reactive power on the voltage level is relatively low, since by injecting a total reactive power of 1116 kVAr in the case of applying the D2 strategy, improvements in voltages of no more than 0.00284 r.u. are obtained.

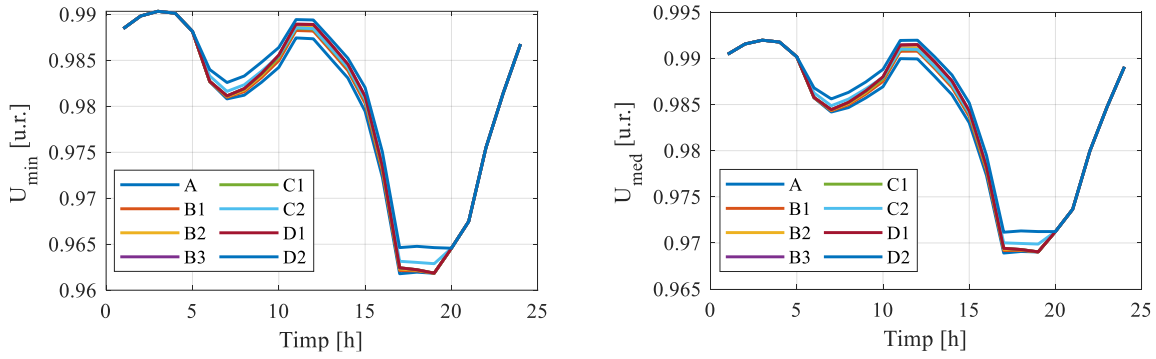

(a) (b)

Figure 4.5. Profile of a) minimum and b) average nodal voltages in the microgrid for May 16th.

The total active power required by *Pcons consumers* is shown in Figure 4.6(a) alongside the total power generated by the Pgen PVPP and the power required by the P_S system microgrid. For the latter, a single curve is presented for all eight strategies considered, as the largest differences between them are less than 1.2%. Figure 4.6 (b) shows the reactive power required by the Q_S microgrid for each control strategy. By applying the control strategies with constant power factor, B1, B2 and B3, a reduction of the reactive power imported by the microgrid at 12 o'clock of 464.5 kVAr, 684.2 kVAr and 875 kVAr is observed, compared to the case with unity power factor. In the case of the C1 and C2 strategies, the total reactive powers required from the system at 12 o'clock are reduced by 524.7 kVAr and 527.9 kVAr, respectively. In the case of the optimal control strategy with conventional limits, D1, the Q_S curve overlaps the curve

B3, while in the case of the optimal control strategy with extended limits, D2, the Q_S value at 12 o'clock is reduced by 976.95 kVAr compared to strategy A. Also, in the D2 strategy, the Q_S values are negative in the range 6 – 13, with values between –25 kVAr and –2.9 kVAr.

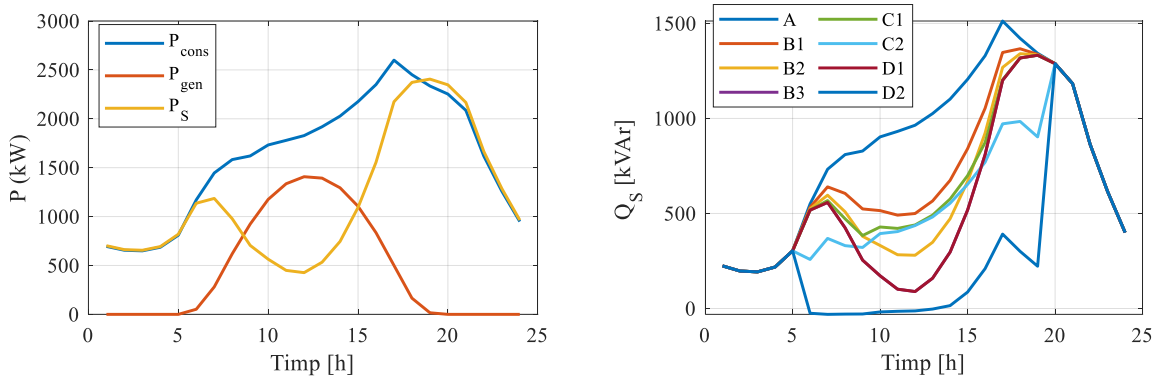

(a) (b)

Figure 4.6.: a) The balance of active power at the level of the microgrid and the reactive power imported by the microgrid from the system, for the day of 16th of May.

Figures 4.7 (a) and (b) show the hourly profiles of total active power losses at the level of the ΔP microgrid, respectively their average daily values, for the eight strategies considered. Based on the two figures, it can be seen that the highest values of power losses are obtained in the case of applying strategy A. At 12 o'clock, when the power delivered by the PVPPs is maximum, the ΔP values are reduced from 16.37 kW (strategy A), by 58.3% to 6.83 kW, by 73.3% to 4.37 kW and by 79.8% to 3.3 kW by applying the strategies with constant power factor B1, B2 and B3, respectively. In the case of the C1 and C2 local reactive power compensation strategies, the power losses are reduced by 62.9% and 63.2% compared to the values obtained in the case of strategy A, up to 6.07 kW and 6.03 kW. The extended limits considered in the D2 optimal control strategy allow a reduction in active power losses at 12 o'clock of 81.4%, up to 3.04 kW. The highest values of the average daily active power losses of 36,26 kW are observed in the case of the application of strategy A, and by applying strategy D2 they are reduced to 26,62 kW.

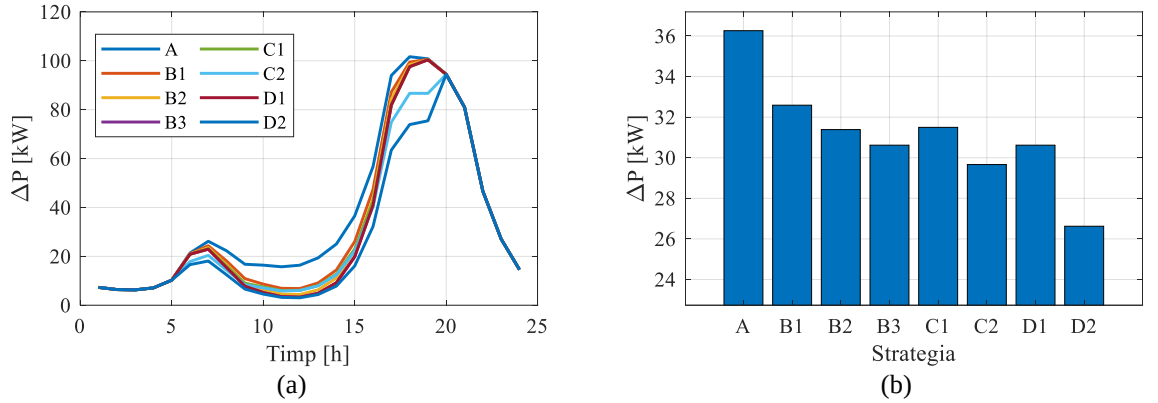

(a) (b)

Figure 4.7.: a) Hourly profile of power losses and b) average daily power losses in the microgrid for 16th of May.

4.3.2. 6th of June

The second day selected for the analysis of the operation of the microgrid is June 6th, when a high consumption is recorded simultaneously with the average value of the power generated by the photovoltaic plants. From the point of view of consumption, the day of June 6th ranks in

the first 6% days of the year with the highest consumption, and the power generated by PVPPs is very close to the average annual value.

Based on the values presented in figure 4.8 (b), it is observed that the application of strategy A leads to obtaining the highest values of average daily power losses of 49.3 kW. Their values are reduced by 6.2%, 8.6% and 10.4% by applying strategies B1, B2 and B3, respectively by 9.6% and 16.3% in the case of strategies C1 and C2 and by 10.4 %, respectively 24.5% in the case of optimal control strategies D1 and D2.

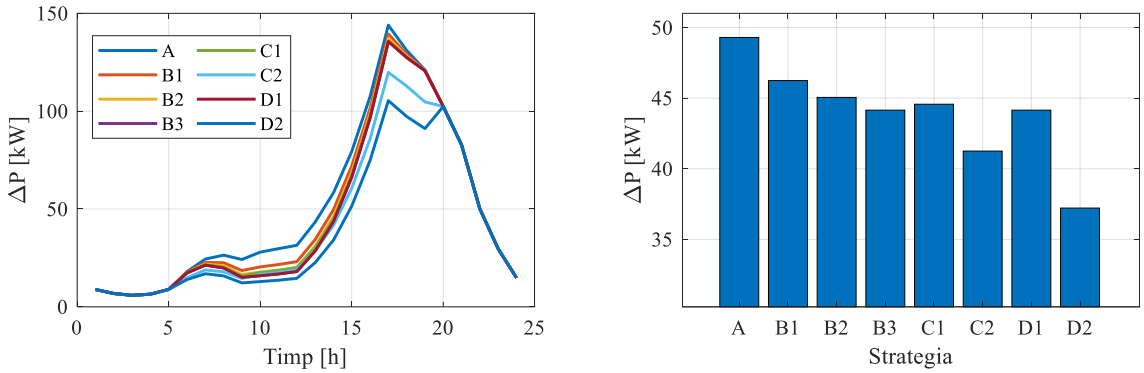

(a) (b)

Figure 4.8.: a) Hourly profile of power losses and b) average daily power losses in the microgrid for June 6th.

4.3.3. 26th of June

The third day selected in this study, namely June 26, when high values of the power demanded by consumers are recorded, at the same time as low values of the power generated by photovoltaic plants. From the point of view of consumption, the selected day falls into the first 10% days with the highest consumption, and from the point of view of the power generated by photovoltaic plants, it ranks in the top 10% with the lowest values.

The hourly profiles of the total active power losses ΔP and their average daily values are shown in Figures 4.9 (a) and (b) for the eight strategies considered. From the point of view of average losses during the day of June 26th , by applying type B strategies, a reduction of up to 5.4% can be observed compared to the reference level of 48.7 kW obtained in strategy A. In the case of strategies with extended limits, the largest reductions in losses are obtained of 14.8% in the case of C2 and 22.15% in the case of D2.

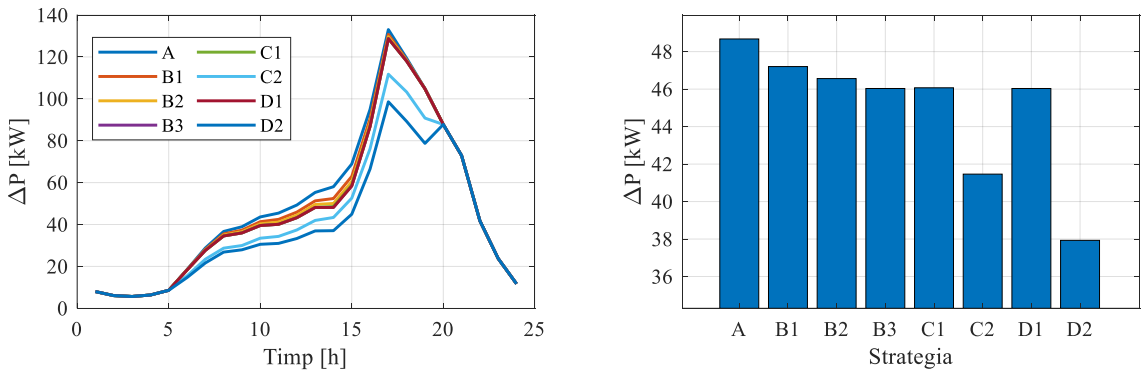

(a) (b)

Figure 4.9: a) Hourly profile of power losses and b) average daily power losses in the microgrid for 26th of June.

4.3.4. 9th of April

This sub-chapter presents the fourth selected day, namely April 9th , when high values of the power generated by photovoltaic power plants and low values of the power demanded by consumers are recorded simultaneously. April 9th falls in the first 3% days with the highest power generated, and in terms of consumption, also in the first 3% days with the lowest values.

The hourly profiles of the total active power losses ΔP are shown in Figure 4.10 (a) and their daily average values in Figure 4.10 (b). Also, in the case of April 9th , the highest values of power losses are obtained in the case of the application of strategy A, and the lowest in the case of the optimal control strategy with extended limits D2.

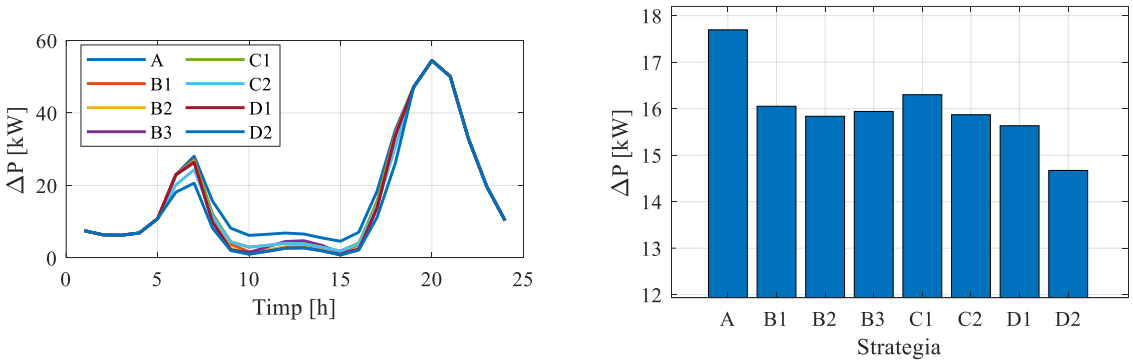

(a) (b)

Figure 4.10: a) Hourly profile of power losses and b) average daily power losses in the microgrid for 9th of April.

4.3.5. Analysis of the operation during one year

This chapter presents an analysis of the functioning of the microgrid in the context of the application of the eight strategies for controlling the reactive power during one year.

Figure 4.11(a) shows a boxplot graph of the reactive power values imported by the microgrid from the system, but only for the hours when the photovoltaic plants are operating. First of all, it can be seen that the median value higher than 792.9 kVAr is obtained in the case of applying strategy A, when the power factor is unitary. In the case of strategies B1, B2 and B3, the median values are reduced to 616.6 kVAr, 543.0 kVAr, respectively 473.3 kVAr, representing a reduction of 22.2%, 31.5% and 40.3% respectively compared to the value obtained in strategy A, considered as a reference. The reactive power compensation strategies demanded by local consumers with conventional limits C1 and extended limits C2 lead to the reduction of the median values of Q_{sl} to 545.2 kVAr and 400.5 kVAr, which represents a reduction of 31.2% and 49.5% respectively relative to strategy A. By applying the optimal control strategy with conventional limits D1, the median value is 47.3 kVAr, reduced by 40.3% compared to strategy A. In the case of considering the extended limits, the optimization algorithm determines a median value of –26.4 kVAr, which represents an export of reactive power from the microgrid to the system. Secondly, the minimum values of Q_{sl} are negative in all type B, C and D strategies, with the most negative minimum value of Q_{sl} of – 544.8 kVAr obtained in the case of strategy B3, when the power factor is 0.85. Moreover, in the case of the optimal control strategy with extended limits D2, it is observed that the quartile values of 75% and 25% are very close, namely – 4.9 kVAr and – 39.7 kVAr. By comparison, in the case of applying strategy A, the related values are 971.9 kVAr and 689.7 kVAr.

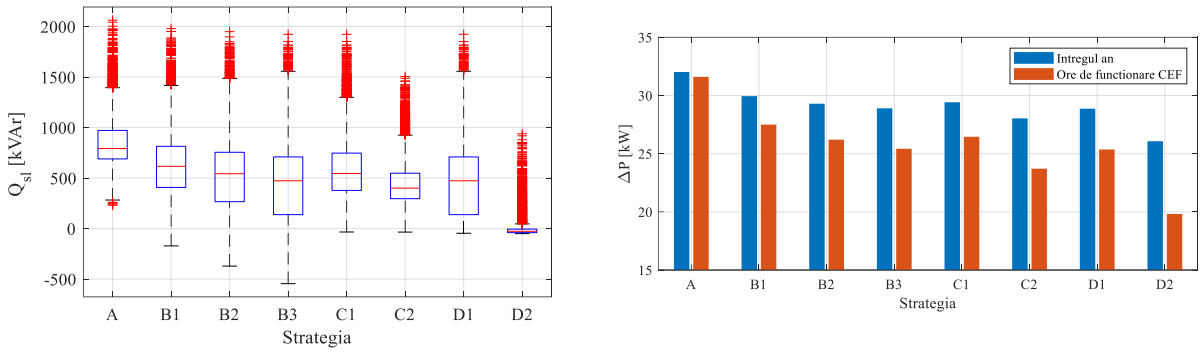

(a) (b)

Figure 4.11. a) Boxplot representation for the required power from the system of the microgrid and b) average annual values of power losses.

The average active power losses across the microgrid are shown in Figure 4.11(b) for the eight reactive power control strategies. Figure 4.11(b) shows two sets of data: the average power losses for the whole year, with the vertical bars in blue, and the average values obtained only during the hours when the photovoltaic plants are operating, with the bars in red. In the case of operating the power plants at unity power factor, the average values of losses for the whole year are 32 kW, and in the case of applying type B strategies, with constant power factor, the values are reduced to 29.9 kW, 29.3 kW and 28.9 kW, representing a variation of 6.6%, 8.45 and 9.7% compared to the reference values obtained in strategy A. By applying the local compensation strategies C1 and C2, the average values at the entire level per year are reduced by 8.1% when conventional limits are considered and 12.5% when extended limits are applied, while optimal control strategies D1, with conventional limits, and D2, with extended limits, losses are reduced by 9.7% and 18.4%, respectively. If only the time intervals in which the photovoltaic plants operate are considered, it can be seen that in the case of strategy A the average power losses are 31,6 kW, and in the case of strategies B1, B2 and B3 these values are reduced by 13 %, 17,1 % and 19,6 %. Local compensation strategies lead to the reduction of power losses during the hours when photovoltaic plants operate by 16.5% when conventional reactive power limits are considered, respectively by 25% when extended limits are considered. The lowest average values of power losses are obtained by applying the optimization algorithm with conventional and extended limits. Thus, in the case of strategies D1 and D2, the average power losses are reduced to 25,4 kW and 19,8 kW respectively, representing a reduction of 19,6 % and 37,3 % respectively compared to the reference values obtained in strategy A. Also, by applying the extended reactive power limits within the optimisation algorithm, a reduction in the average power losses during the operating hours of the is observed by 22 % compared to the situation considered conventional limits.

CHAPTER 5. CONCLUSIONS

5.1. General conclusions

The doctoral thesis is part of the current research topics on the integration of photovoltaic power plants in the control of reactive power, especially due to the current context of accelerated development of renewable energy sources.

The main objective of the doctoral thesis is the optimal control of the reactive power generated by photovoltaic power plants in order to minimize the total losses of active power in a microgrid. For this, two optimization problems were formulated and solved in the two case studies with the help of metaheuristic algorithms.

In the first case study, the optimal control of the reactive power in a microgrid was achieved with the help of capacitor banks and photovoltaic power plants. The objective function consisted of minimizing active power losses while respecting the operational limits of the control devices and the microgrid. In the first part of the case study, five metaheuristic algorithms were tested in order to select the best performing of them. For this, 50 consecutive runs were made for the Gray Wolf Algorithm, the Sine-Cosine Algorithm, the Genetic Algorithm, the Particle Swarm Optimization and the Swarm of Swarm Algorithms. In conclusion, the Gray Wolf Algorithm was chosen because it achieved the best numerical results in the 50 consecutive runs. In the second part of this case study, the Gray Wolf Algorithm was used to optimize the reactive power for 15 scenarios obtained by generating all combinations between three consumption scenarios (peak load, base mode and off-peak load) and five production scenarios (considering the power generated by the plants at 0%, 25%, 50%, 75% and 100% of the rated power). As the purpose of this study is the integration of photovoltaic power plants in the reactive power control, the reference scenarios were defined in the assumption of using exclusively capacitor banks, while the plants operate at unity power factor. The results obtained proved a significant reduction in active power losses at the microgrid level, up to 34.8% in the off-peak load scenario, up to 30.5% in the peak load scenario and up to 31.3% in the base load scenario. These reductions are due to the more uniform distribution of reactive power sources in the microgrid, the continuous control carried out by inverters (compared to the stepwise control of capacitor banks), but also to the quantitative contribution in the peak load scenario, when capacitor banks do not have sufficient reactive power. In conclusion, the integration of photovoltaic power plants into reactive power control, along with existing devices such as capacitor banks, has led to improved microgrid operating modes by significantly reducing power losses.

In the second case study, we aimed to achieve the control of the reactive power in the microgrid exclusively on the basis of photovoltaic plants. For this case study, hourly consumption and production curves were used for the duration of an entire calendar year. Eight reactive power control strategies were applied: Unity power factor (strategy A), constant power factor equal to 0.95, 0.90 and 0.85 (strategies B1, B2 and B3), local compensation of reactive power with ordinary or extended limits (strategies C1 and C2) and optimal control of reactive power with ordinary or extended limits (strategies D1 and D2). The local compensation involved the operation of the power plants in order to fully cover the reactive power consumption of the consumers connected to the same bus as the power plant. The usual limits applied in the C1 and C2 strategies consisted of applying the minimum power factor to the active power generated, while in the case of extended limits, it was applied to the nominal power. In the first part of the study, the analysis of the functioning of the microgrid in the eight control strategies was carried out during four relevant days, and in the second part, a summary of the operation of the entire calendar year was presented. In conclusion, it emerged that the optimal control strategies (D1 and D2) give the best results by achieving a continuous and centralized control during each time slot. By comparison, strategy A with unity power factor does not provide any reactive power support, and those with constant power factor (B1, B2 and B3) can generate excess reactive power at lunchtime when production is maximum and consumption is relatively low, and in the morning and afternoon hours generate an insufficient

amount of reactive power. The local reactive power compensation strategies (C1 and C2) have generated better results, but they only take into account local loads, not the situation at the level of the entire microgrid. From the point of view of the reactive power limits, the results proved that in the case of considering the usual limits, the optimization algorithm has a sufficient adjustment band only at lunchtime, therefore the positive impact on the operation of the microgrid is also limited outside this time slot. In conclusion, by applying the optimization strategy with consideration of extended limits, significant reductions in power losses of up to 37.3% were achieved throughout the year.

5.2. Personal contributions

Personal contributions are presented below:

(i) Conducting bibliographic studies on photovoltaic power plants, microgrids, their steady-state calculation and metaheuristic algorithms.

(ii) Formulation of optimization problems to minimize active power losses by controlling the reactive power generated by 1) capacitor banks and photovoltaic plants and 2) exclusively by photovoltaic plants.

(iii) Realization of a software for the calculation of the load flow of the microgrid in the presence of photovoltaic plants in Matlab, implementation of optimization problems formulated in Matlab codes and their use together with the existing codes of metaheuristic algorithms.

(iv) Realization of the case study entitled "Integration of photovoltaic plants in the optimal control of reactive power within a microgrid"

- Modeling the microgrid and defining multiple scenarios based on the powers generated and consumed in the microgrid;
- Made a comparison between the performances of five different metaheuristic algorithms: the Gray Wolf Algortim, the Algortim of the Swarm of Salpi, the Particle Swarm Optimization, the Sine-Cosine Algorithm and the Genetic Algortim, in solving the formulated optimization problem;
- Determination of optimal values for capacitor banks steps and for the reactive power generated by photovoltaic power plants and analysis of the results obtained

(v) Realization of the case study entitled "Optimal reactive power in a microgrid exclusively based on photovoltaic power plants":

- Modeling the microgrid and defining hourly curves of production and consumption for the duration of an entire calendar year.
- Determination of the optimal values for the reactive power generated by photovoltaic power plants for each day during a calendar year.
- Analysis of the results obtained for four representative days, respectively of a synthesis of the results for the entire calendar year.

(vi) Dissemination of the results obtained through two journal articles rated ISI (Revue Roumaine des Sciences Techniques and the Scientific Bulletin of UNSTPB) and two international conference articles (International Symposium on Advanced Topics in Electrical Engineering – ATEE 2023 and 2022 International Conference and Exposition on Electrical And Power Engineering EPE).

5.3. Further research proposals

The research presented within the doctoral thesis can be continued by addressing the following themes:

- Increasing the complexity of the mathematical model by introducing more controllable devices such as: new wind, diesel or gas turbine energy sources, consumers with controllable devices or storage systems
- Extension of the analysis to include the impact on the distribution network feeding the studied microgrid
- Making a comparison between the performance of metaheuristic and classical optimization algorithms.

SELECTIVE BIBLIOGRAPHY

[1] *S. Gorjian, P. E. Campana* (ed.), Solar Energy Advancements in Agriculture and Food Production Systems, Academic Press, 2022.

[2] *L. Li, J. Tu, Y. Yang, J. Wu, K. Hu, S. Yu,* Effect of finger interruption mode on the performance of crystalline silicon solar cells, Solar Energy Vol. 238, 15 mai 2022, pag. 381-391.

[3] *M. Yaich, Y. Dhieb, et al*., Metaheuristic Optimization Algorithm of MPPT Controller for PV system application, E3S Web of Conferences, vol. 336, 2022.

[4] *S. Panda, s.a.*, Investigating the similarities and differences between front and back surface cooling for PV panels, Materials Today Proceedings, Nr. 74, Vol. 5, 2022.

[5] *I. Triștiu*, Impactul Generării Distribuite, Facultatea de Energetică, Universitatea Națională de Știință și Tehnologie Politehnica din București, Note de curs, 2024.

[6] National Renewable Energy Laboratory (NREL), Microgrids, disponibil on-line la https://www.nrel.gov/grid/microgrids.html [accesat în 1 iulie 2024].

[7] *M. Eremia* (ed.), *et. al*. – Electric Power Systems: Vol. 1 Electric networks, Publishing House of the Romanian Academy, Bucharest, 2006.

[8] *A. D. Rana, J. B. Darji, Mosam Pandya – Backward / Forward Sweep Load Flow Algorithm for Radial Distribution System*, International Journal for Scientific Research & Development (IJSRD), Vol. 2, Nr. 01, 2014, ISSN (online): 2321-0613.

[9] *Paulo M. De Oliveira-De Jesus*, A Simplified Formulation for the Backward/Forward Sweep Power Flow Method, arXiv:2010.06389.

[10] *R. Berg, E.S. Hawkins, W.W. Pleines*, Mechanized Calculation of Unbalanced Load Flow on Radial Distribution Circuits, IEEE Transactions on Power Apparatus and Systems , Vol. PAS-86, Nr. 4, pag. 415-421, 1967.

[11] *U. Eminogl, M. H. Hocaoglu*, Distribution Systems Forward/Backward Sweep-based Power Flow, Algorithms: A Review and Comparison Study, Electric Power Components and Systems, Vol.37, Nr. 1, Pag. 91-110, 2008.

[12] *U. Eminogl, M. H. Hocaoglu,* Distribution Systems Forward/Backward Sweep-based Power Flow, Algorithms: A Review and Comparison Study, Electric Power Components and Systems, Vol.37, Nr. 1, Pag. 91-110, 2008.

[13] *Xu Jingzhou, Chen Xiao*, Forward/backward sweep method based on map structure for power flow calculation of distribution system, China International Conference on Electricity Distribution (CICED) 2010), Nanjing, China, 2010.

[14] TF C6.04.02 : TB 575 Benchmark Systems for Network Integration of Renewable and Distributed Energy Resources, CIGRE, 2014.

[15]. *J. A. M. Rupa, S. Ganesh*, Power flow analysis for radial distribution system using backward/forward sweep method, World Acad. Sci. Eng. Technol. Int. J. Elect. Comput. Eng., 8(10), pp. 1621-1625, 2014.

[16]. *D. O. Sidea, I. I. Picioroaga, C. Bulac*, Optimal Battery Energy Storage System Scheduling Based on Mutation-Improved Grey Wolf Optimizer Using GPU-Accelerated Load Flow in Active Distribution Networks, IEEE Access, 9, pp. 13922-13937, 2021.

[17]. *S. Mirjalili, S. M. Mirjalili*, A. Lewis, Grey wolf optimizer, Advances in engineering software, 69, pp. 46-61, 2014.

[18]. *H. Faris, I. Aljarah, M.A. Al-Betar, S. Mirjalili*, Grey wolf optimizer: a review of recent variants and applications, Neural computing and applications, 30, 2, pp. 413-435, 2018.

[19] *D. O. Sidea, A.M. Tudose, I.I. Picioroagă, L. Toma, C. Bulac*, "Adapted Grey Wolf Optimizer for Dynamic Economic Dispatch in a Hybrid Microgrid", 10th International Conference on ENERGY and ENVIRONMENT (CIEM), 14-15 October 2021, Bucharest, Romania.

[20] *J. H. Holland*, "Adaptation in natural and artificial systems", The U. of Michigan Press 1975.

[21] *J. Kennedy, R. Eberhart*. "Particle swarm optimization." Proceedings of ICNN'95-international conference on neural networks. Vol. 4. IEEE, 1995, Perth, Australia.

[22]. *X. Zhang, Z. Wang, Z. Lu*, Multi-objective load dispatch for microgrid with electric vehicles using modified gravitational search and particle swarm optimization algorithm, Applied Energy, 306, A, pp. 118018, 2022.

[23]. *S. Mirjalili*, SCA: A Sine Cosine Algorithm for Solving Optimization Problems, Knowledge-Based Systems, 96, pp. 120-133, 2016.

[24]. *A. B. Gabis, Y. Meraihi, S. Mirjalili, A. Ramdane-Cherif*, A comprehensive survey of sine cosine algorithm: variants and applications, Artificial Intelligence Review, 54, pp. 5469-5540 2021.

[25]. *A. C. Pérez-Flores, J. D. M. Antonio, V. H. Olivares-Peregrino, H. R. Jiménez-Grajales, A. Claudio-Sánchez, G. V. G. Ramírez*, Microgrid Energy Management With Asynchronous Decentralized Particle Swarm Optimization, IEEE Access, 9, pp. 69588-69600 (2021).

[26] *S. Mirjalili, A.H. Gandomi, S.Z. Mirjalili, S. Saremi, H. Faris, S.M. Mirjalili*, Salp Swarm Algorithm: A bio-inspired optimizer for engineering design problems", Adv. Eng. Softw., Vol. 114, 2017, pp. 163–191.

[27] ***M. Burlacu***, *V. Năvrăpescu, A. Chirilă, D. Deaconu*, Optimal Reactive Power Management for Microgrids Based on Photovoltaic Inverters using Sine-Cosine Algorithm, Revue Roumaine des Sciences Techniques, Série Électrotechnique et Énergétique, Vol. 67, Nr. 2, 2022.

[28]. Twenpower Medium-Voltage XLPE Cables Catalogue, disponibil on-line la: https://t3.lappcdn.com/fileadmin/DAM/Miltronic_Sweden/4_Servicecenter/2Nedladdningscenter/TKF_Twenpower_Medium_Voltage.pdf [accesat în 2022].

[29] ***M. Burlacu***, *V. Năvrăpescu*, Performance analysis of metaheuristic algorithms for optimal reactive power control in microgrids, 2022 International Conference and Exposition on Electrical And Power Engineering (EPE), Iasi, Romania, 2022.

[30] *K. A. Khan, S. Shafiq, M. Khalid*, "A Strategy for Utilization of Reactive Power Capability of PV Inverters", 9th International Conference on Power and Energy Systems (ICPES), Perth, Australia, 2019.

[31] *H. Li, K. H. Chao, L. L. Li*, Research on Inverter Integrated Reactive Power Control Strategy in the Grid-Connected PV Systems, Energies, 10(7), pp. 912, 2017.

[32]. *M. Farivar, R. Neal, C. Clarke, S. Low*, Optimal Inverter VAR Control in Distribution Systems with High PV Penetration, 2012 IEEE Power and Energy Society General Meeting, San Diego, USA, 2012.

[33] *A. Cabrera-Tobar, E. Bullich-Massague, M. Aragues-Penalba, O. Gomis-Bellmunt*, Active and Reactive Power Control of a PV Generator for Grid Code Compliance, Energies, 12(20), pp. 3872, 2019.

[34] ***M. Burlacu***, *V. Năvrăpescu*, Operational Analysis of PV Inverter Reactive Power Control Strategies for Microgrids, U.P.B. Scientific Bulletin, Seria C, Vol. 84, Nr. 4, 2022.

[35] *W. Peng, Y. Baghzouz, S. Haddad*, Local Load Power Factor Correction by Grid-Interactive PV Inverters, 2013 IEEE Grenoble Conference, Grenoble, France, 2013.

[36] Sandia National Laboratories, Reactive Power Capability and Interconnection Requirements for PV and Wind Plants", disponibil on-line la https://www.esig.energy/wiki-main-page/reactive-power-capability-and-interconnection-requirements-for-pv-and-wind-plants/ [accesat în 13 martie 2022].

[37] ***M. Burlacu***, *V. Năvrăpescu*, Impact Analysis of Optimal Photovoltaic Power Plant Reactive Power Control upon Microgrids Operation, 2023 13th International Symposium on Advanced Topics in Electrical Engineering (ATEE), București, România, 2023.

[38] . U.S. Department of Energy, Simulated Load Profiles for DOE Commercial Reference Buildings (17 Years Using NSRD Data), disponibil on-line la: https://openei.org/datasets/dataset/ simulated-load-profiles-17year-doe-commercial-reference-buildings [accesat în 13 martie 2022].

[39]. *S. Pfenninger, I. Staffell*, Long-term patterns of European PV output using 30 years of validated hourly reanalysis and satellite data, Energy, 114, pp. 1251–1265, 2016.